

UC Davis

UC Davis Previously Published Works

Title

Evaluating the Water Cycle Over CONUS at the Watershed Scale for the Energy Exascale Earth System Model Version 1 (E3SMv1) Across Resolutions

Permalink

<https://escholarship.org/uc/item/4bv1h8v1>

Journal

Journal of Advances in Modeling Earth Systems, 15(11)

ISSN

1942-2466

Authors

Harrop, Bryce E
Balaguru, Karthik
Golaz, Jean-Christophe
et al.

Publication Date

2023-11-01

DOI

10.1029/2022ms003490

Copyright Information

This work is made available under the terms of a Creative Commons Attribution-NonCommercial-NoDerivatives License, available at
<https://creativecommons.org/licenses/by-nc-nd/4.0/>

Peer reviewed














RESEARCH ARTICLE

10.1029/2022MS003490

Evaluating the Water Cycle Over CONUS at the Watershed Scale for the Energy Exascale Earth System Model Version 1 (E3SMv1) Across Resolutions

Key Points:

- The water cycle slows down (decreased fluxes) when grid spacing has a four times refinement
- HR generally improves evapotranspiration, but precipitation and other terms have mixed results
- HR improves precipitation extremes, storm event precipitation contributions, and mountain snowpack

Bryce E. Harrop¹ , Karthik Balaguru¹ , Jean-Christophe Golaz² , L. Ruby Leung¹ , Salil Mahajan³ , Alan M. Rhoades⁴ , Paul A. Ullrich⁵ , Chengzhu Zhang² , Xue Zheng² , Tian Zhou¹ , Peter M. Caldwell² , Noel D. Keen⁴, and Azamat Mametjanov⁶

¹Pacific Northwest National Laboratory, Richland, WA, USA, ²Lawrence Livermore National Laboratory, Livermore, CA, USA, ³Oak Ridge National Laboratory, Oak Ridge, TN, USA, ⁴Lawrence Berkeley National Laboratory, Berkeley, CA, USA, ⁵Department of Land, Air, and Water Resources, University of California-Davis, Davis, CA, USA, ⁶Argonne National Laboratory, Lemont, IL, USA

Supporting Information:

Supporting Information may be found in the online version of this article.

Correspondence to:

B. E. Harrop,
bryce.harrop@pnnl.gov

Citation:

Harrop, B. E., Balaguru, K., Golaz, J.-C., Leung, L. R., Mahajan, S., Rhoades, A. M., et al. (2023). Evaluating the water cycle over CONUS at the watershed scale for the Energy Exascale Earth System Model version 1 (E3SMv1) across resolutions. *Journal of Advances in Modeling Earth Systems*, 15, e2022MS003490. <https://doi.org/10.1029/2022MS003490>

Received 7 NOV 2022
Accepted 16 OCT 2023

Abstract The water cycle is an important component of the earth system and it plays a key role in many facets of society, including energy production, agriculture, and human health and safety. In this study, the Energy Exascale Earth System Model version 1 (E3SMv1) is run with low-resolution (roughly 110 km) and high-resolution (roughly 25 km) configurations—as established by the High Resolution Model Intercomparison Project protocol—to evaluate the atmospheric and terrestrial water budgets over the conterminous United States (CONUS) at the large watershed scale. The warm season water cycle slows down in the HR experiment relative to the LR, with decreasing fluxes of precipitation, evapotranspiration, atmospheric moisture convergence, and runoff. The reductions in these terms exacerbate biases for some watersheds, while reducing them in others. For example, precipitation biases are exacerbated at HR over the Eastern and Central CONUS watersheds, while precipitation biases are reduced at HR over the Western CONUS watersheds. The most pronounced changes with resolution to the water cycle come from reductions in precipitation and evapotranspiration. The reduction in evapotranspiration reduces the biases across nearly all of the CONUS. Additional exploratory metrics show improvements to water cycle extremes (both in precipitation and streamflow), fractional contributions of different storm types to total precipitation, and mountain snowpack.

Plain Language Summary This study seeks to better understand how the U.S. DOE's Earth system model, Energy Exascale Earth System Model, simulates the conterminous United States (CONUS) water cycle. To accomplish this goal, we examine the atmosphere and land water budget terms at the watershed and seasonal space and time scales. At higher resolution and during the warm season, all of the terms in the water budget become smaller: precipitation, evapotranspiration, moisture convergence, and runoff. The reductions in evapotranspiration lead to improvements over nearly the entire CONUS, while other terms show mixed results when increasing resolution. We also examine exploratory metrics with expected resolution sensitivity—including precipitation and streamflow extremes, storm events, and snowpack—and find modest improvements.

1. Introduction

The water cycle is a key component to many facets of life. Hence better understanding of the water cycle is a key science goal of the development of the Energy Exascale Earth System Model (E3SM) to address U.S. Department of Energy (DOE) mission needs related to climate change impacts on energy production and use (Leung et al., 2020; Zamuda et al., 2013). In particular, we seek to answer the question, “how does better resolving features important to the water cycle at the watershed scale improve the representation of freshwater supplies at that scale?” At the watershed scale, important climatic features generated by complex topography, land surface cover and land use, and other surface heterogeneity and their interactions with atmospheric circulation are not well captured at the standard resolution (110 km) used in E3SM (J. Golaz et al., 2019). We expect some of these features to improve by increasing the horizontal resolution of the component models, which can lead to improvements in the overall simulation of the water cycle. Quantifying the sensitivity of the water cycle to resolution in E3SMv1 is the primary goal of this manuscript.

© 2023 Battelle Memorial Institute. Oak Ridge National Laboratory et al. and The Authors. Journal of Advances in Modeling Earth Systems published by Wiley Periodicals LLC on behalf of American Geophysical Union.

This is an open access article under the terms of the [Creative Commons Attribution-NonCommercial-NoDerivs License](https://creativecommons.org/licenses/by/4.0/), which permits use and distribution in any medium, provided the original work is properly cited, the use is non-commercial and no modifications or adaptations are made.

Notice: Manuscript Authored by Battelle Memorial Institute Under Contract Number DE-AC05-76RL01830 with the US Department of Energy. The US Government retains and the publisher, by accepting this article for publication, acknowledges that the US Government retains a non-exclusive, paid-up, irrevocable, world-wide license to publish or reproduce the published form of this manuscript, or allow others to do so for US Government purposes. The Department of Energy will provide public access to these results of federally sponsored research in accordance with the DOE Public Access Plan: (<http://energy.gov/downloads/doe-public-access-plan>)

** The submitted manuscript has been created by UChicago Argonne, LLC, Operator of Argonne National Laboratory ("Argonne"). Argonne, a U.S. Department of Energy Office of Science laboratory, is operated under Contract No. DE-AC02-06CH11357. The U.S. Government retains for itself, and others acting on its behalf, a paid-up nonexclusive, irrevocable worldwide license in said article to reproduce, prepare derivative works, distribute copies to the public, and perform publicly and display publicly, by or on behalf of the Government. The Department of Energy will provide public access to these results of federally sponsored research in accordance with the DOE Public Access Plan. <http://energy.gov/downloads/doe-public-access-plan>

Any improvements to the simulated water cycle from increasing horizontal resolution depend on both the scales being resolved as well as the scales being analyzed. For example, Demory et al. (2014) found that the water cycle was sensitive to horizontal resolution down to roughly 60 km (as measured by the ratio of global land to global total precipitation). Vannière et al. (2019) found a similar sensitivity, while also noting (a) global precipitation increases with increasing model resolution and (b) improved seasonal mean circulations lead to improved regional precipitation features. The agreement between results becomes less coherent when the focus shifts from a global to a regional perspective. For example, Monerie et al. (2020) found that simulated precipitation improvements converge around 60 km resolution over northeast Brazil, but improvements over the Andes do not converge even down to 25 km resolution (the highest they tested). Similar scales of resolution (on the order of tens of kilometers) have found improvements to precipitation (e.g., Demory et al., 2020; Schiemann et al., 2018), though these are not uniform (Ito et al., 2020). Ajibola et al. (2020) found that increasing resolution to roughly quarter or half degree grid spacing showed no reliable improvement in rainfall over West Africa. Similarly, for a resolution change of $\sim 1.125^\circ$ to $\sim 0.25^\circ$, Benedict et al. (2019) found improvements for the Rhine region in Europe, but the same improvements were absent in the Mississippi region in North America, highlighting the need for a deeper look at which aspects of the hydrologic cycle are sensitive to which scales in different environments. Relevant to this study, X. Huang and Ullrich (2017) and many previous studies cited therein found increased horizontal resolution ($\sim 0.25^\circ$) improved precipitation over the conterminous United States (CONUS), particularly in the mountainous regions of the Western US. Small et al. (2014) also showed improvements in Rocky Mountain rainfall variability at quarter degree grid spacing relative to one degree grid spacing. Similarly, F. Huang et al. (2020) found model performance in precipitation over the Rocky Mountain region was related to horizontal resolution in the fifth phase of the Coupled Model Intercomparison Project (CMIP5; Taylor et al., 2012) ensemble.

Like mean rainfall, water cycle extremes show improvements with increased horizontal resolution (Bador et al., 2020; Balaguru et al., 2020; X. Huang & Ullrich, 2017; Iorio et al., 2004; Kiehl & Williamson, 1991; Mahajan et al., 2015, 2018, 2022; Rhoades et al., 2021; Schiemann et al., 2018; Srivastava et al., 2020; Terai et al., 2017; M. F. Wehner et al., 2010, 2014; M. Wehner et al., 2021). For the relatively small range of horizontal resolutions found across the CMIP6 (Eyring et al., 2016) ensemble, horizontal resolution is not a good predictor of model performance for rainfall extremes (Akinsanola et al., 2020). Uncertainty in extremes from observations can sometimes be as large as intermodel differences (Bador et al., 2020; Srivastava et al., 2020). Of particular interest, though, are the findings of M. Wehner et al. (2021), which note that typical measures of extreme precipitation increase with horizontal resolution over the CONUS, but carefully constructed model skill metrics that account for resolution do not show significant sensitivity. In other words, a large degree of the sensitivity was related to the metrics calculations themselves instead of improvement from the model. Bador et al. (2020) also note that increased horizontal resolution on its own is not sufficient for systematic improvement in simulating precipitation extremes.

Sharma et al. (2019) point out that increased resolution in regional simulations can easily be disrupted by uncertainties in boundary forcing. In fully coupled global models the boundary conditions are freely evolving according to each model component, which puts greater emphasis on the need for understanding how the system interacts as a whole. With global models, what is considered high resolution is often much coarser than regional models. Even convective-permitting global models (grid spacing on the order of a few kilometers), such as those simulations run as part of DYNAMICS of the Atmospheric general circulation Modeled On Non-hydrostatic Domains (DYAMOND; Stevens et al., 2019), cannot run long enough to provide insight to the seasonal cycle or modes of interannual variability. The High Resolution Model Intercomparison Project (HighResMIP; Haarsma et al., 2016) was proposed to organize a common framework for models (both coupled and uncoupled alike) to assess resolution sensitivity on simulated climate processes. E3SM high- and low-resolution experiments have been run generally consistent with the HighResMIP protocol. There are two deviations from the HighResMIP protocol worth noting: (a) E3SM uses prognostic aerosols instead of the prescribed values suggested for HighResMIP; and (b) the control simulations (from which the transient simulations used herein are branched) follow a different initialization procedure for the ocean (documented in Section 2.5 of Caldwell et al., 2019).

The approach taken for this manuscript is to examine the CONUS seasonal water cycle at the level 2 Hydrologic Unit Codes (HUC2) watershed scale. We aim to quantify the biases in the terms important for the water budget in both the atmosphere and land, as well as the sensitivity of these biases to resolution at the scales used in the HighResMIP experimental design. Further analyses allow us to quantify the factors leading to changes in the

moisture budget terms. We will show that the CONUS water cycle slows down at higher resolution with all terms in the moisture budget decreasing in magnitude from low to high resolution.

Many additional metrics can be used to gain insight into the simulated water cycle. Pendergrass et al. (2020) suggested a series of “exploratory metrics” for the water cycle that can aid in understanding its behavior. Some of these we anticipate having sensitivity to horizontal resolution and we will examine them within this manuscript. These include investigating precipitation unevenness distributions, storm events (including tropical cyclones (TCs), extratropical cyclones (ETCs), and atmospheric rivers (ARs)), extreme precipitation, extreme streamflow, and snowpack. Many of these features are also critical needs for water resource management.

This manuscript serves two primary functions. First, it provides a quantitative assessment of the simulated water cycle over the CONUS in E3SM at two resolutions for the seasonally varying components of the water budget in both the atmosphere and land. The second is to identify which other aspects of the water cycle are sensitive to resolution in E3SM using several exploratory metrics. The manuscript is organized in the following manner. Section 2 details the key features of the simulations used. Section 3 examines the response to increasing resolution of the global water cycle over land. Section 4 examines the seasonal water cycle at the watershed scale and quantifies changes to the biases in the model owing to resolution. Section 5 details additional metrics to examine further sensitivities in the simulated water cycle to resolution changes in E3SM. Finally, in Section 6, we summarize the findings of this study and make recommendations for future work.

2. Experimental Design

The simulations used in this study are fully coupled and follow the experimental design described in Caldwell et al. (2019) with one primary difference: the simulation pair does not use repeating 1950 conditions, but instead uses transient forcings following the HighResMIP (Haarsma et al., 2016) protocol for the years spanning 1950 through 2014. Analysis of these simulations is done using the final 30 years of each simulation (1985–2014). Individual coupled simulations like these raise a question about the role of long-term variability in assessing aspects of the water cycle over the CONUS region. While a large ensemble and long pre-industrial control simulations exist for E3SMv1, they use a different set of tuning parameters relative to the experiments examined in this manuscript, requiring an additional level of caution for interpreting results compared between the two. Additionally, our focus is only on demonstrating changes to the long-term mean seasonal cycle between the HR and LR simulations, which 30 years of simulation data should be sufficient to cover. We reproduce a selection of the salient features of the E3SMv1 model design here to aid in understanding this particular manuscript. More thorough descriptions may be found in J. Golaz et al. (2019) and Caldwell et al. (2019).

The atmosphere component is described in detail by Rasch et al. (2019) and its cloud and convective characteristics are analyzed by Xie et al. (2018). It is based on the spectral-element dynamical core (Dennis et al., 2012) with 72 vertical levels. The following processes are parameterized: deep convection (Zhang-McFarlane; Neale et al., 2008; Richter & Rasch, 2008; G. J. Zhang & McFarlane, 1995); macrophysics, turbulence, and shallow convection (Cloud-Layers Unified by Binormals; J.-C. Golaz et al., 2002; Larson & Golaz, 2005; Larson, 2017); microphysics (Morrison-Gottelman Version 2; Gottelman & Morrison, 2015; Gottelman et al., 2015); aerosol treatment (four-mode Modal Aerosol Model; Liu et al., 2016; Wang et al., 2020); and radiative transfer (Rapid Radiative Transfer Model for general circulation models; Mlawer et al., 1997; Iacono et al., 2008).

The ocean and sea ice components use the Model for Prediction Across Scales (MPAS; Petersen et al., 2019; Ringler et al., 2013). A mesoscale eddy parameterization (Gent-McWilliams; Gent & McWilliams, 1990) is used only for the low-resolution simulation (it is disabled for the high-resolution). The mesoscale eddy parameterization used for the LR experiment may not exactly mimic the impact of the resolved eddies in HR and may result in important differences in the ocean circulation. Nevertheless, testing these features is beyond the scope of the current manuscript. Neither the high-resolution nor the low-resolution configurations use a submesoscale eddy transport scheme.

The land model is nearly identical to its parent model, the Community Land Model version 4.5 (Oleson et al., 2013), run with satellite phenology and non-prognostic carbon and nitrogen representation. There are 10 soil layers in the land model. The Model for Scale Adaptive River Transport (MOSART, H. Li et al., 2013; H. Y. Li et al., 2015) is used for river transport (in its grid-based representation). Given runoff simulated by the land

Table 1
Grid Comparisons for the High-Resolution (HR) and Low-Resolution (LR) Configurations of the Model

Grid	atm/land $\sim\Delta x$ (km)	atm/ land # of columns	Ocean/sea ice $\sim\Delta x$	Ocean/sea ice # of columns	River $\sim\Delta x$	River # of columns
HR	25	777,602	8–16 km	3,693,225	0.125°	4,147,200
LR	110	48,602	30–60 km	235,160	0.5°	259,200

model, MOSART explicitly simulates channel velocity, channel water depth, and water surface area following a simplified form of the one-dimensional Saint-Venant equation.

Both the high-resolution (HR) and low-resolution (LR) configurations examined herein share the same tuning parameter values. In other words, our LR configuration mirrors that of the “LRtunedHR” simulation described and used in Caldwell et al. (2019). As a consequence, the LR configuration analyzed here differs from the standard E3SMv1 (J. Golaz et al., 2019). We chose this approach to focus on the impact of resolution, rather than different tuning choices.

There are three separate grids used for both the HR and LR configurations for the five components (the atmosphere and land share one grid, the ocean and sea ice share one grid, and the river transport model uses its own grid). Table 1 lists the key grid differences between the HR and LR configurations. The atmosphere and land are on a cubed sphere grid, the ocean and sea-ice use Spherical Centroidal Voronoi Tessellations, and the river model uses a regular lat-lon mesh. The vertical levels for all components are the same between the two resolutions except for the ocean model (80 levels for HR and 60 levels for LR). The river model provides freshwater input to the ocean.

To satisfy numerical stability requirements at higher resolution requires a shorter model time step to run the simulations. Table 2 shows the time steps used for the various components for each resolution. As in Caldwell et al. (2019), our analyses for model resolution sensitivities convolve both the resolution sensitivity and the time step sensitivity, and while we generally use terminology such as “resolution sensitivity” throughout this manuscript, it has been shown that the time step sensitivity can be as large or larger than the resolution sensitivity in some instances (Jung et al., 2012).

The HighResMIP protocol calls for pseudo-equilibrium 1950 repeating conditions as the control run from which to branch the transient experiments. Because the 1950 conditions are not exactly in equilibrium, the model drifts throughout the ~ 50 years of simulation. As the model state drifts, simulated sea surface temperature biases become larger in magnitude. Therefore, to minimize the biases in the model state at the beginning of the transient period, the transient runs branch off near the beginning of the control runs analyzed by Caldwell et al. (2019). We use the earliest available restart point, 5 years after initialization for the HR configuration and 10 years after initialization for the LR configuration.

We are interested in assessing the water cycle at the watershed scale. To that end, we focus our analysis on the hydrologic unit maps, which we will refer to by their hydrologic unit code level 2 (HUC2) demarcation (see

Figure 1 for a map of the HUC2 watersheds and Table 3 for a list of watershed names). The HUC2 basins are adapted by the U.S. Geological Survey (USGS) from those established by Seaber et al. (1987). There are 18 HUC2 basins covering the CONUS. The boundaries of these basins are marked on map plots throughout this manuscript. While there are higher-level HUC categories denoting smaller hydrologic regions of the CONUS, the horizontal spatial resolution of the LR simulation is insufficient to resolve these features to make for a fair comparison against the HR simulation.

To analyze the model output at the watershed scale, we generate mapping files using TempestRemap (Ullrich & Taylor, 2015; Ullrich et al., 2016) for both model grids onto each HUC2 watershed region. We also generate mapping files for each observational product onto each HUC2 watershed region. These mapping files are then used to remap the monthly timeseries of the moisture budget terms from the model and observations onto the HUC2 watershed regions. We use these monthly timeseries to quantify the biases in each moisture budget term. To quantify uncertainties, the model output and data are grouped by month of the year; the mean is the average across all years, and each year is treated as an independent sample for statistical tests and confidence intervals. To test the statistical significance of differences

Table 2
Time Steps Used in the High-Resolution (HR) and Low-Resolution (LR) Configurations

Time step (minutes)	HR	LR
atm dynamics and advection	1.25	5
atm physics-dynamics coupling	15	30
ocn	6	10
ocn barotropic	0.2	0.67
Ice dynamics	7.5	15
Ice thermodynamics	15	15
River	60	60
atm/ice/land coupling	15	30
ocn coupling	30	30
River coupling	180	180

Note. Additional time step details can be found in Table 2 of Caldwell et al. (2019).

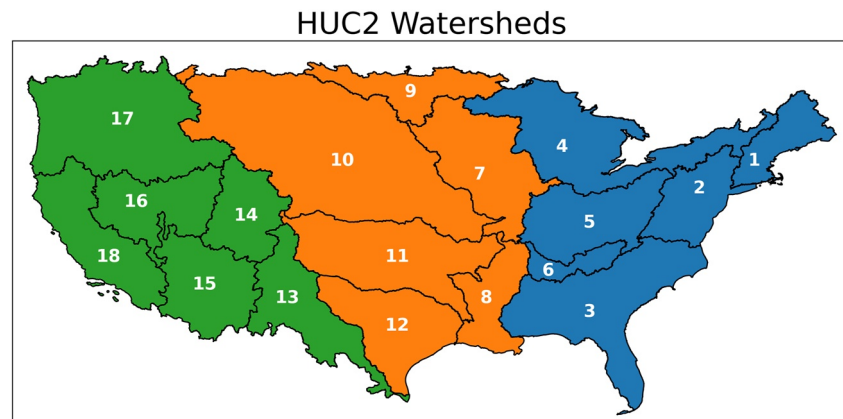


Figure 1. Hydrologic Unit Codes watershed map. We refer to watersheds 1–6 (in blue) as the Eastern conterminous United States (CONUS), watersheds 7–12 (in orange) as the Central CONUS, and watersheds 13–18 (in green) as the Western CONUS.

at the watershed level, *t*-tests are computed using all available years for each observational data set, and for all 30 years of the model output.

A number of observational products are used to quantify the biases in the simulations. For precipitation, we use the Global Precipitation Climatology Project (GPCP) one-degree daily (1DD) data for years 1997–2017 (Huffman et al., 2001, 2009) and the Tropical Rainfall Measuring Mission (TRMM) 3B43 data for years 1998–2013 (Huffman et al., 2007). For evapotranspiration (ET), we use the Derived Optimal Linear Combination Evapotranspiration (DOLCE) data (<https://doi.org/10.4225/41/58980b55b0495>) for years 2000–2009 (Hobeichi et al., 2018), the Global Land Evaporation Amsterdam Model (GLEAM) data for years 1980–2018 (Martens et al., 2017; Miralles et al., 2011), and the MODerate Resolution Imaging Spectroradiometer (MODIS) data for years 2000–2014 (De Kauwe et al., 2011; Mu et al., 2011). Note that the DOLCE data are not independent of the other ET data, as that data set combines six different ET products, including the GLEAM and MODIS data. For terrestrial water storage anomaly we use the Gravity Recovery and Climate Experiment (GRACE) data for the years 2002–2014 (Swenson & Wahr, 2006). For runoff we use a 1/16th degree daily runoff database generated by the Variable Infiltration Capacity (VIC) hydrologic model over CONUS for years 1985–2011 (Livneh et al., 2013). The VIC runoff was forced by a gridded daily near-surface observed meteorological data (Livneh et al., 2013). Livneh et al. (2013) compared the VIC runoff to observed and naturalized flows and found the VIC runoff does a good job representing these flows (see their Figure 5).

3. Global Land Analysis

Before analyzing the CONUS water budget, it is useful to examine the biases over land in several climate metrics, as well as their response to increasing horizontal resolution. Figure 2 shows biases for precipitation, evapotranspiration, 2 m air temperature, surface net radiative flux, and surface wind speed for JJA. Figure 3 shows the same patterns, but for DJF.

Panels a–d of Figure 2 show the precipitation as measured by GPCP, the biases for both HR and LR, and the difference (HR minus LR). The overall bias pattern is quite similar between HR and LR with prominent features like the dry biases over the Eastern CONUS, Amazon, and Europe being present at both resolutions. Consistent with the previous studies outlined in the Introduction, the precipitation response to increasing resolution is not

Table 3

Names of the Hydrologic Unit Codes Watersheds

HUC2	Watershed name
01	New England
02	Mid Atlantic
03	South Atlantic-Gulf
04	Great Lakes
05	Ohio
06	Tennessee
07	Upper Mississippi
08	Lower Mississippi
09	Souris-Red-Rainy
10	Missouri
11	Arkansas-White-Red
12	Texas-Gulf
13	Rio Grande
14	Upper Colorado
15	Lower Colorado
16	Great Basin
17	Pacific Northwest
18	California

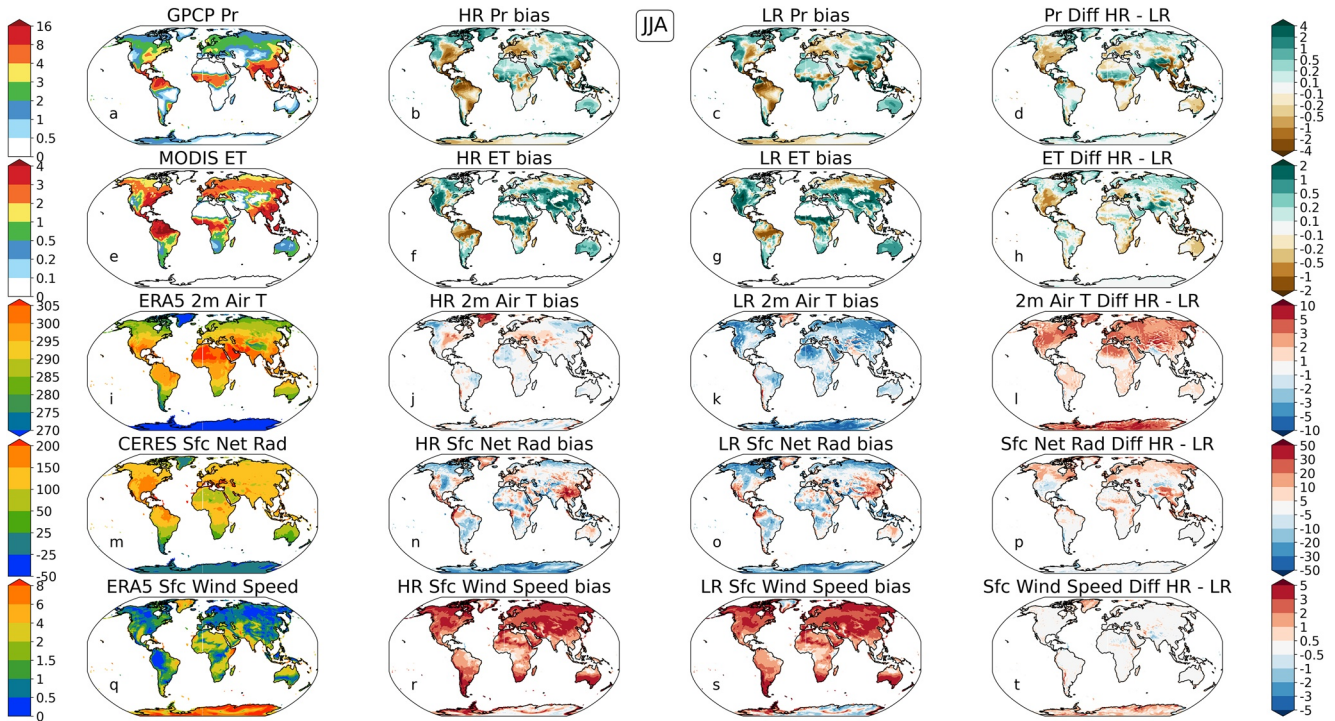


Figure 2. (Top row) precipitation, (second row) evapotranspiration, (third row) 2 m air temperature, (fourth row) surface net radiation), and (fifth row) near-surface wind speed for the (left column) reference data, (second column) HR bias, (third column) LR bias, and (fourth column) difference between HR and LR. Precipitation and evapotranspiration are provided in units of mm/day, temperature is in units of K, surface net radiation is in units of W/m^2 , and wind speed is in units of m/s.

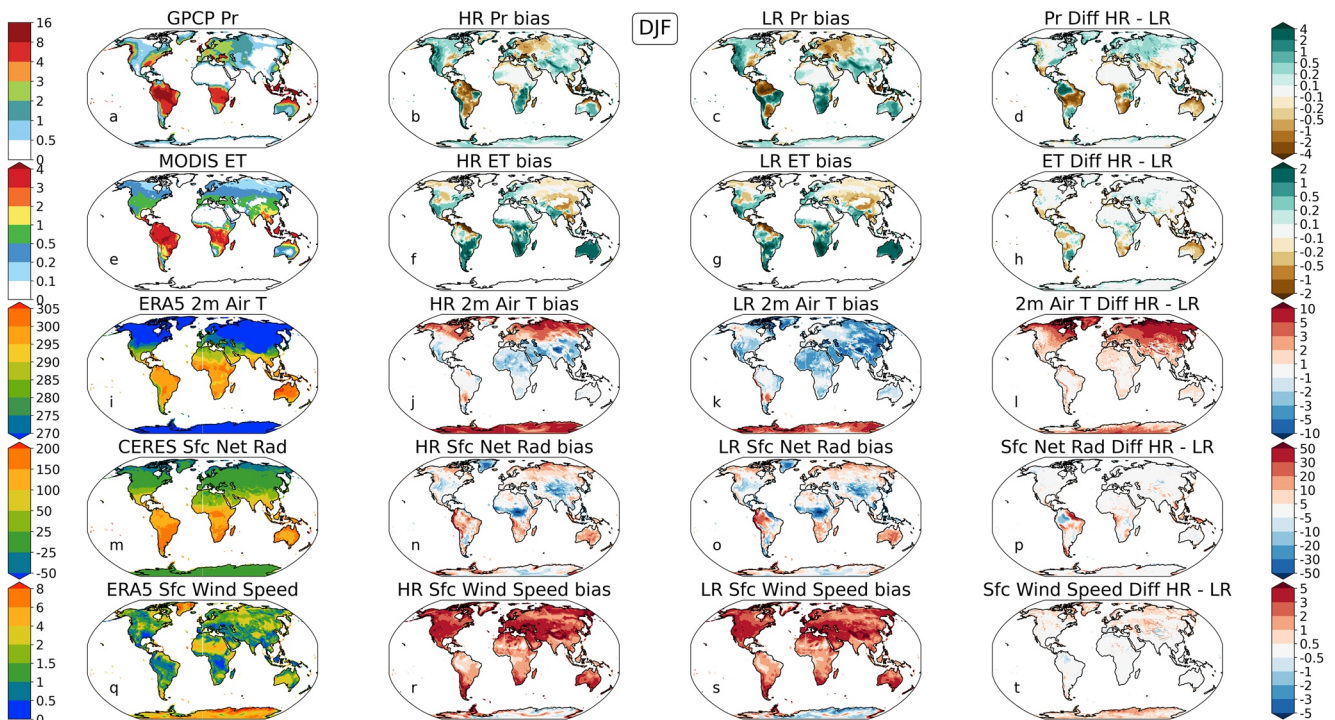


Figure 3. Same as Figure 2, but for the DJF season.

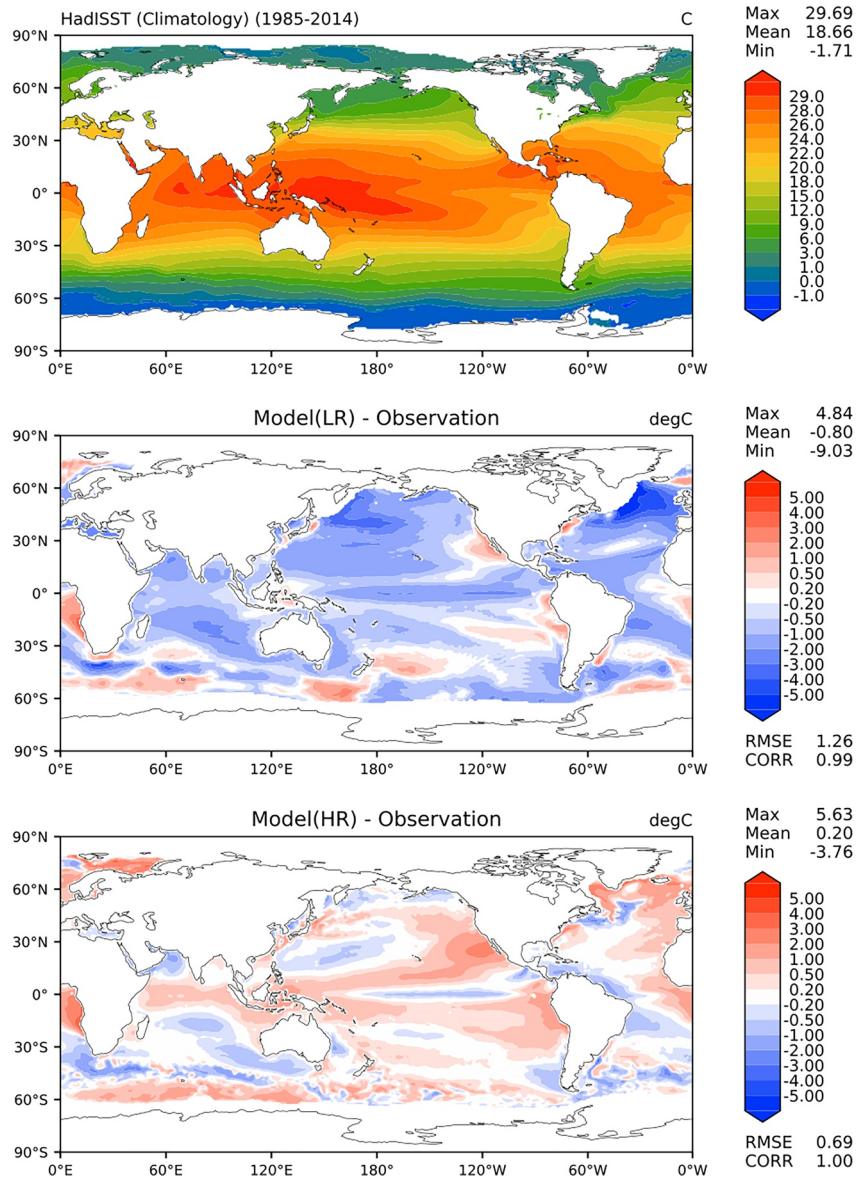


Figure 4. Comparison between observed global SST to LR and HR simulations for Annual (ANN) mean. Top figures show ANN mean from the Hadley Center Global Sea Ice and Sea Surface Temperature (HadISST); Middle (LR) and bottom (HR) figures show simulated minus observed values.

uniform over land. The CONUS shows a decrease in precipitation, but there are numerous other regions that show increases in precipitation. One example is over the Indian monsoon region, which shows the largest precipitation change by magnitude.

Panels e–h of Figure 2 are the same as panels a–d, but for evapotranspiration. Like precipitation, the overall bias pattern is qualitatively similar between HR and LR. The ET differences between HR and LR show good spatial coherence with the precipitation changes, suggesting a close coupling of the response of surface moisture fluxes to resolution. This spatial coherence is less apparent during the DJF season (Figure 3 panels d and h), particularly over South America.

Panels i–l of Figure 2 show the 2 m air temperature biases and response to increasing resolution. LR has a prominent cold bias over land that is substantially reduced for HR. The warming over land is consistent with a global increase in SSTs in HR compared to LR (see Figure 4).

Panels m–p of Figure 2 show the net surface radiation (positive values denote a net downward flux). Like precipitation and ET, the bias patterns are qualitatively similar in HR and LR. The difference pattern shows an increase in surface net radiation at the high northern latitudes in JJA. Much of the CONUS shows a decrease in surface net radiation. In DJF (Figure 3) most of the resolution sensitivity for surface net radiation is seen in the Southern Hemisphere, as expected since insolation and surface temperatures are both generally at their largest values during local summer.

Finally, panels q–t of Figure 2 show the surface wind speed. There is virtually no response of the windspeed over land to resolution changes. The biases are virtually identical in both the HR and LR, with both showing much stronger winds than those in ERA5. These biases persist, regardless of season (JJA or DJF).

4. CONUS Water Budget and Its Sensitivity to Resolution

The atmospheric water budget can be written as follows.

$$\partial_t S_{\text{atm}} + \nabla \cdot \{\mathbf{v}q\} = E - P \quad (1)$$

where $\partial_t S_{\text{atm}}$ is the time-tendency of atmospheric water storage, \mathbf{v} is the horizontal wind vector, q is the specific humidity, curly braces denote a column integral, P is surface precipitation, and E is surface evapotranspiration. At the scales of interest for this study, changes in atmospheric moisture tendency ($\partial_t S_{\text{atm}}$) are orders of magnitude smaller than the other terms at the time and space scales examined here, and we neglect that term for our analyses. Therefore, the land surface water budget can be written as follows.

$$\partial_t S_{\text{stc}} = P - E - R \quad (2)$$

where $\partial_t S_{\text{stc}}$ is the time-tendency of surface water storage (including soil moisture, snowpack, and groundwater), and R is runoff (combined surface and sub-surface).

As described in the introduction, we seek to quantify the biases and resolution sensitivity of the terms in the moisture budget (Equations 1 and 2) at the watershed scale and for the seasonal cycle. The HUC2 watersheds represent natural boundaries for the water cycle in the land and also make for an ideal level of granularity to use for this study as both LR and HR model grids can resolve each basin.

Even restricting the spatial and temporal scales, there are several aspects that need to be quantified. First, we aim to quantify the biases in the E3SM at LR against observations and ERA5 reanalysis (Hersbach et al., 2020). While reanalyses like ERA5 are still modeling products, ERA5 has the advantage over other observations of consistency between its water cycle budget terms. Here, “consistency” means that the moisture budget is expected to have a small residual relative to collecting terms from observations. For the spotlight diagrams shown in the following section, we have done the analysis both with and without ERA5 for precipitation, evapotranspiration, terrestrial water storage anomaly, and runoff, and found no changes to our conclusions. We only show the analyses that include ERA5. Second, we aim to quantify any changes to the water budget terms between LR and HR. Where differences arise, we then assess whether these differences are improvements or degradations to the simulation. We perform these analyses for each month of the year and each watershed in the CONUS, and then make spotlight diagrams to summarize the results.

4.1. Seasonal Watershed Water Cycle Budget

A summary for precipitation is presented in Figure 5. Each row denotes a different HUC2 watershed basin and each column represents a month of the year. The numbers are the mean difference in E3SM across resolution (HR-LR). The cells of the table are colored depending on the relationship between E3SM across resolutions, and with the observational and reanalysis products used to evaluate them. White denotes a month where no significant bias exists between either LR or HR with the observations. Yellow denotes months where no significant difference exists between LR and HR, but both are significantly biased relative to observations. Purple denotes months where LR is biased relative to observations, while HR is not (the amelioration of a previous bias). Green denotes months where LR is biased relative to observations and HR makes a significant improvement upon that bias (i.e., HR is still biased relative to observations, but the magnitude of that bias is significantly lower than in LR). Orange denotes the opposite of green—both LR and HR are biased against observations, but the bias is

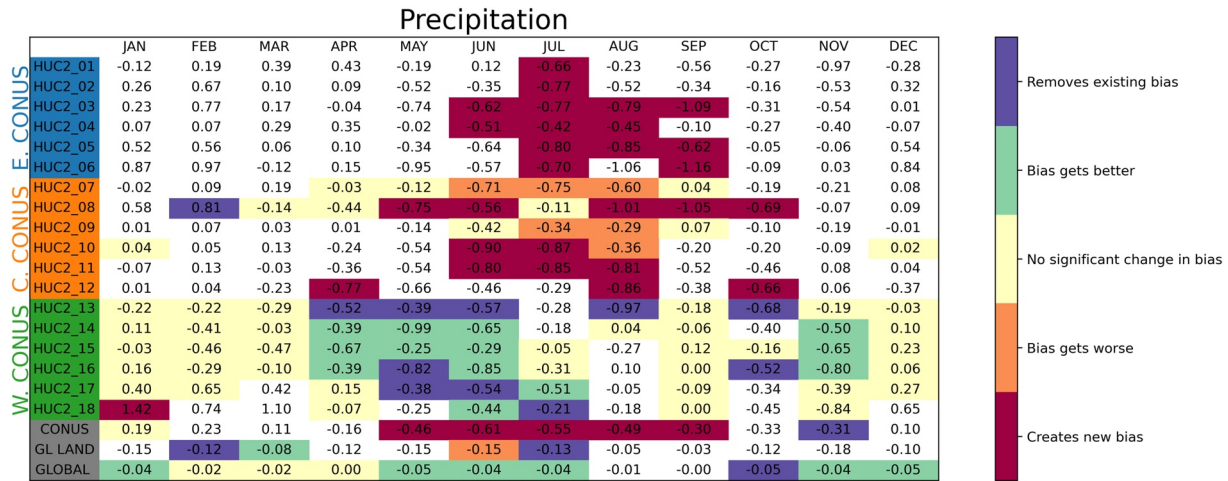


Figure 5. Stoplight diagram for precipitation. Each column represents a month. The first 18 rows each represent a Hydrologic Unit Codes watershed, “CONUS” is the CONUS mean, “GL LAND” is the global land (northward of 60°S) mean, and “GLOBAL” is the global mean. The values in each cell are the mean difference between LR and HR (HR-LR). White denotes a month where no significant bias exists between either LR or HR with the observations. Yellow denotes months where no significant bias exists between LR and HR, but both are significantly biased relative to observations. Purple denotes months where LR is biased relative to observations, while HR is not. Green denotes months where LR is biased relative to observations and HR makes a significant improvement upon that bias. Orange denotes the opposite of green—both LR and HR are biased against observations, but the bias is significantly larger in LR. Finally, red denotes regions where no bias exists for LR, but a bias does occur for HR. Statistical significance is determined using a two-tailed Student’s *t*-test with a 95% significance threshold and treating each year as an independent sample for a particular basin and month. Comparison data sets for precipitation include Global Precipitation Climatology Project, Tropical Rainfall Measuring Mission, and ERA5. Units are in mm/day.

significantly larger in HR than in LR. Finally, red denotes regions where no bias exists for LR, but a bias does occur for HR (the creation of a new bias). Again, for all differences, statistical significance is determined using a two-tailed Student’s *t*-test (with a 95% significance threshold) and treating each year as an independent sample for a particular watershed and month. A value for a particular month and watershed is only considered significant if the test rejects the null hypothesis between the model and all observational and reanalysis products. For example, if the model is considered significantly biased for precipitation, it means the bias is significant between the model and GPCP, the model and TRMM, and the model and ERA5. This approach means months and watersheds where observational products disagree are more likely to be colored white. For example, even though there are some large changes in wintertime precipitation for the Southeast US (consistent with Bacmeister et al., 2014), few cells show any significant change (Figure 5). To facilitate discussion, we group the watershed basins into three broader regions: Eastern CONUS (HUC2 basins 1–6), Central CONUS (HUC2 basins 7–12), and Western CONUS (HUC2 basins 13–18).

Figure 5 shows that for the Eastern CONUS, summertime precipitation biases are created when transitioning from LR to HR. In the fall, winter, and spring, there are no significant precipitation biases for the model at either resolution. For the Central CONUS, a similar degradation in precipitation is found for the summer months. The primary difference between the Eastern and Central CONUS regions is the presence of significant biases for the Central CONUS in the LR configuration.

For the Western CONUS, there are significant improvements in the precipitation, primarily in the late spring and early summer months. When comparing HR and LR, the precipitation response to increasing resolution is consistently negative across the Eastern, Central, and Western CONUS. Similar reductions transitioning from LR to HR were shown by Chang et al. (2020) using the Community Earth System Model (CESM) version 1.3. The bias responses hinge on whether biases exist at LR. For the Eastern and Central CONUS, the precipitation reduction leads to new or exacerbated biases, while for the Western CONUS, the precipitation reduction leads to reduced biases.

Figures 6–9 show the same breakdown as Figure 5, only for the surface evapotranspiration, atmospheric moisture convergence, terrestrial water storage anomaly tendency, and runoff (combined surface and sub-surface), respectively. Figures S1–S5 in Supporting Information S1 provide the full seasonal timeseries for each experiment and data set. Like precipitation, ET decreases across virtually all watersheds when going from LR to HR. The changes

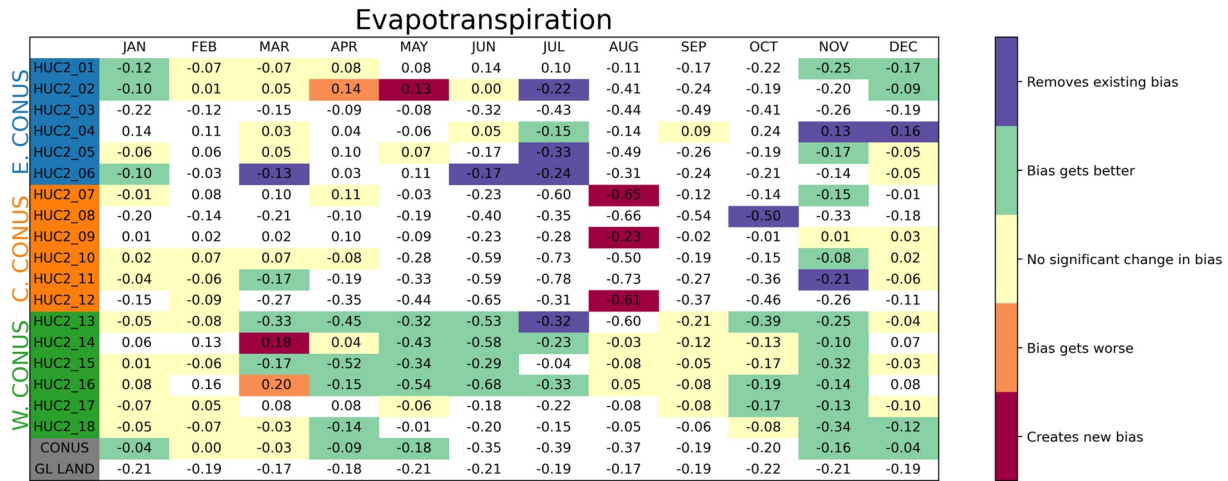


Figure 6. As in Figure 5, but for evapotranspiration. Comparison data sets for evapotranspiration include MODIS, Global Land Evaporation Amsterdam Model, Derived Optimal Linear Combination Evapotranspiration, and ERA5. Units are in mm/day.

in biases, however, are not the same between precipitation and ET. For the Eastern CONUS, the reduction in ET leads to reductions or removals of the summertime biases. The Central CONUS, however, still shows some degradation in simulated ET. Closer examination finds that the DOLCE data, despite drawing from data including MODIS and GLEAM, consistently underestimates ET relative to those other two data sets over the Eastern CONUS making it an outlier (Figure S2 in Supporting Information S1). If we reproduce the ET stoplight diagram without the DOLCE data (Figure S6 in Supporting Information S1), we see a more consistent pattern emerge with improvements in late summer ET over the Eastern CONUS, and degradations in late summer ET over the Central CONUS. Both Eastern and Central CONUS show improvement in ET biases from November through January (a signal absent in the precipitation field). The Western CONUS shows the most coherent agreement between precipitation and ET, with reductions in ET resulting in reduced biases for most western watersheds across much of the year.

For the atmospheric moisture convergence (Figure 7) and terrestrial water storage anomaly tendency (Figure 8), the differences tend to be too small relative to interannual variability, such that very few significant differences exist between model (at either resolution) and observations. The mean moisture convergence for the CONUS changes sign throughout the year. In the cold months, there is a net import of water into most watersheds, while in the warm months, the sign flips such that there is a net export of water for most watersheds. As expected from continuity, $E - P$ shows a pattern consistent with the moisture convergence throughout the year (not shown). The net export of moisture during the summer means that the mean circulation provides limited insight into the

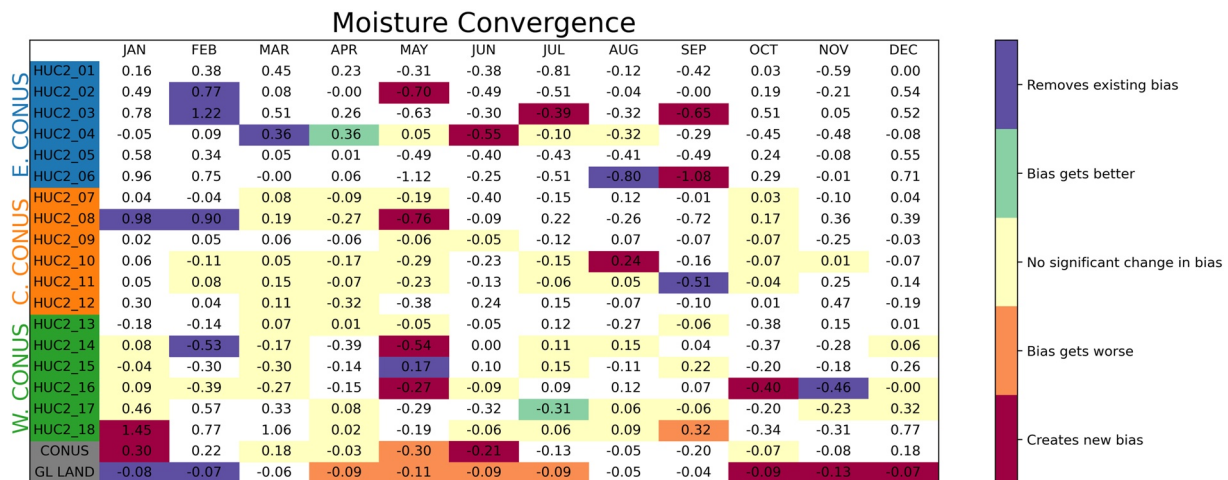


Figure 7. As in Figure 5, but for atmospheric moisture convergence. The comparison data set for moisture convergence is ERA5. Units are in mm/day.

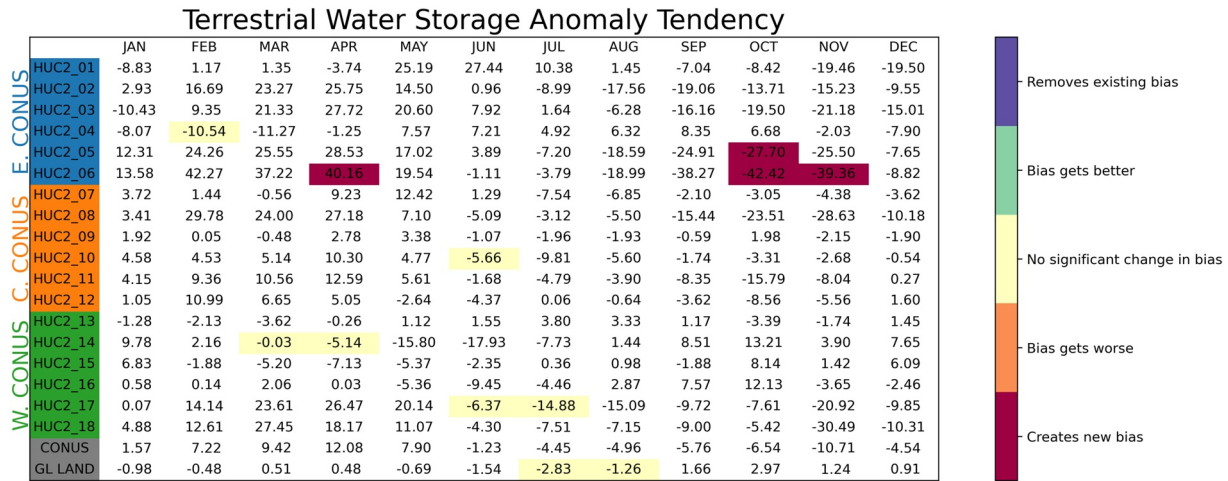


Figure 8. As in Figure 5, but for terrestrial water storage anomaly. Comparison data sets for terrestrial water storage anomaly include Gravity Recovery and Climate Experiment and ERA5. Units are in mm.

precipitation processes for E3SM. Instead, we must examine time-varying circulation patterns. Further examination of such circulations is provided in Section 5.2.

For terrestrial water storage anomaly tendency (Figure 8), the GRACE data record is relatively short compared to the model output, which increases the uncertainty in the observed data. For ERA5, terrestrial water storage anomaly changes are computed as a residual between surface precipitation, ET, and surface plus sub-surface runoff. Somewhat surprisingly, there tends to be a better agreement between the LR and HR model output with the GRACE data than the ERA5 reanalysis (Figure S4 in Supporting Information S1). Despite these differences in the data, the LR and HR model results are statistically indistinguishable from one another over nearly all months and watersheds.

Finally, for the runoff term, the patterns of improvement and degradation over the Central and Western CONUS reflect the changes seen in precipitation (Figure 9) only spread out over more months. In other words, the degradation in Central CONUS runoff is likely linked to the degradation in precipitation. Likewise, the improvement in Western CONUS runoff is likely linked to the improvement in precipitation. For the Eastern CONUS, there is little consistency in the response to changing resolution across watersheds and even across seasons within the same watershed. The Great Lakes watershed is the exception for the Eastern CONUS, with simulated runoff degraded in HR from June through December.

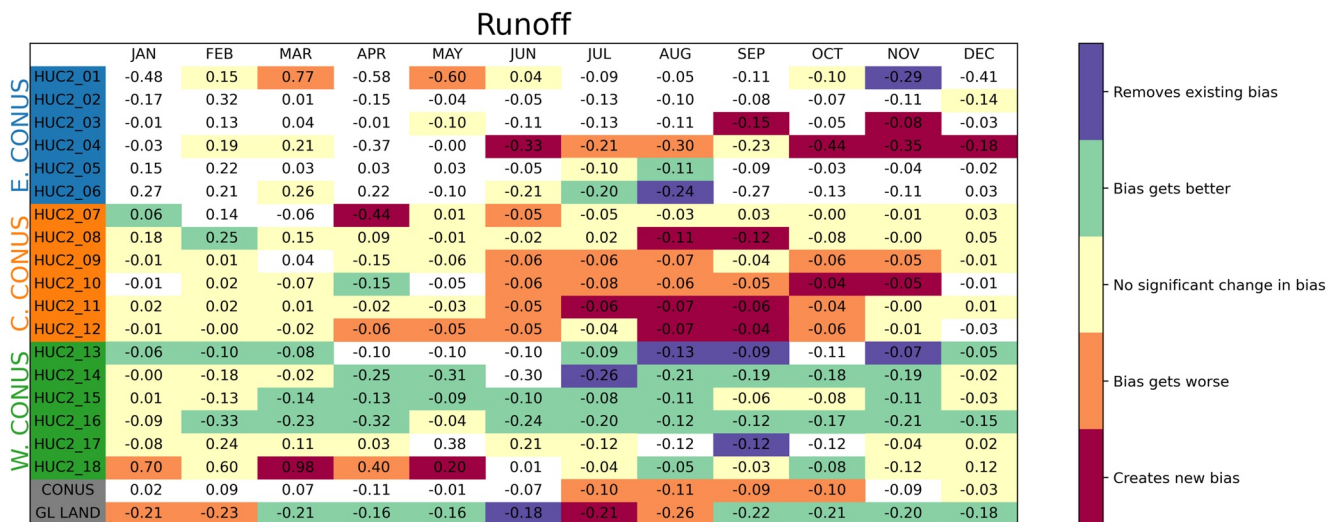


Figure 9. As in Figure 5, but for runoff. Comparison data sets for runoff include Variable Infiltration Capacity and ERA5. Units are in mm/day.

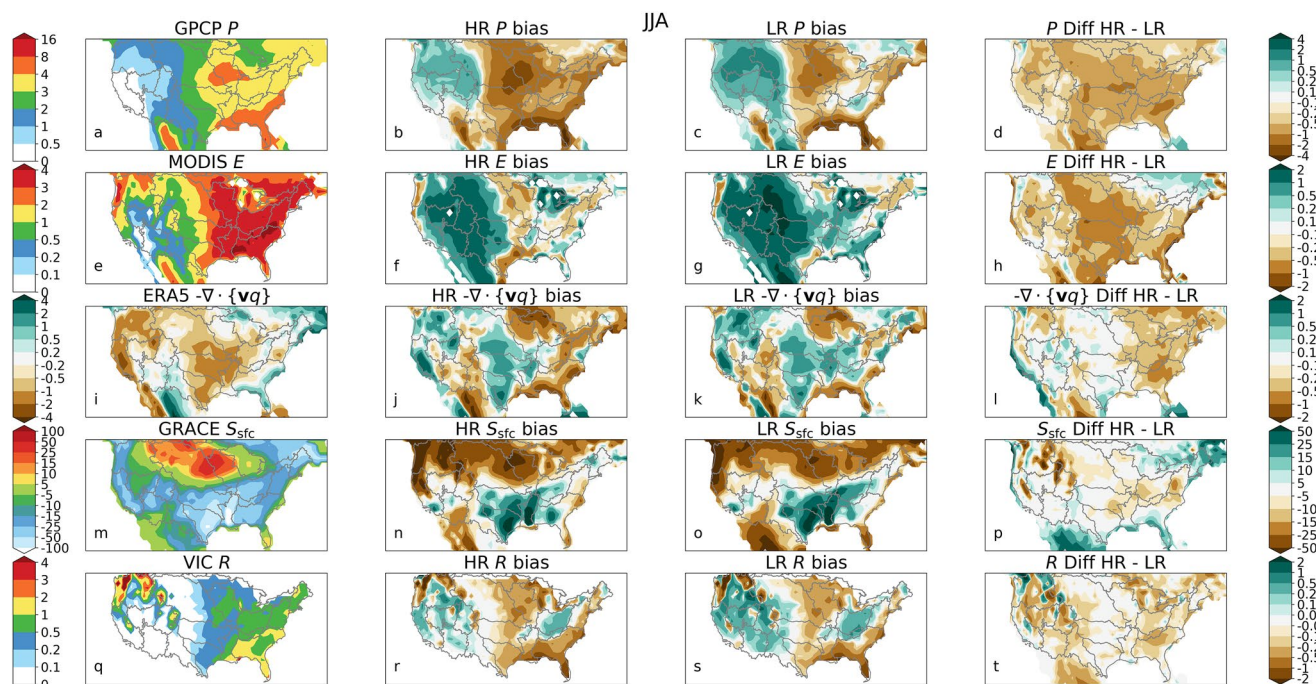


Figure 10. Each of the metrics (precipitation, evapotranspiration, atmospheric moisture convergence, terrestrial water storage anomaly, and runoff) shown for the reference (left-most column), HR and LR bias (second and third columns, respectively), and HR and LR difference (HR minus LR). All values have units of mm/day, except for terrestrial water storage anomaly, which has units of mm.

For all five components (precipitation, ET, moisture convergence, terrestrial water storage anomaly tendency, and runoff) summertime values all decrease going from LR to HR. The differences, however, are only statistically significant for precipitation, ET, and runoff when examining individual months and watersheds. This reduction in precipitation and evapotranspiration coincides with a significant increase in precipitable water and a reduction in soil moisture in HR relative to LR (Figure S7 in Supporting Information S1). While it is unclear whether either of these facts is the cause of the other, it is valuable for framing the changes to individual moisture budget terms, as we will discuss in more detail later. Each of the spotlight diagrams show the CONUS and global land averages (precipitation also shows the global average) and the decrease in these metrics at higher resolution is still seen across these larger spatial averages. Though there is substantial cancellation across regions (as can be seen in Figures 2 and 3) the consistency across CONUS and the global land suggests that the changes over CONUS are not unique to that region.

4.2. Warm Season Changes

Figure 10 shows a map of these metrics for the JJA season. Figure 10 shows that the decline in precipitation is broadly uniform across the Eastern and Central CONUS, while being a little weaker over the Western CONUS. This regional difference is because of the selected season being plotted. If we were to plot AMJJ, the decline in precipitation would be greater over the Western CONUS (not shown). Compared to metrics like terrestrial water storage anomaly and runoff, the precipitation sensitivity to the better-refined topography is somewhat weak during JJA. In DJF, as can be seen in Figure 3d there is much more precipitation sensitivity to orography over the Western CONUS, possibly owing to more orographically forced precipitation in local winter.

Figure 10 shows the decrease in ET between HR and LR is stronger over the central CONUS than either the Eastern or Western CONUS regions. Again, the principal difference between the precipitation and ET differences is that the decrease in ET leads to improvements relative to observed ET because the LR had large positive biases. It is important to point out that there are some limitations with the simulated ET in these experiments. Transpiration accounts for more than half of ET (Lian et al., 2018) but the use of satellite phenology potentially limits the sensitivity of transpiration, and hence ET, to resolution.

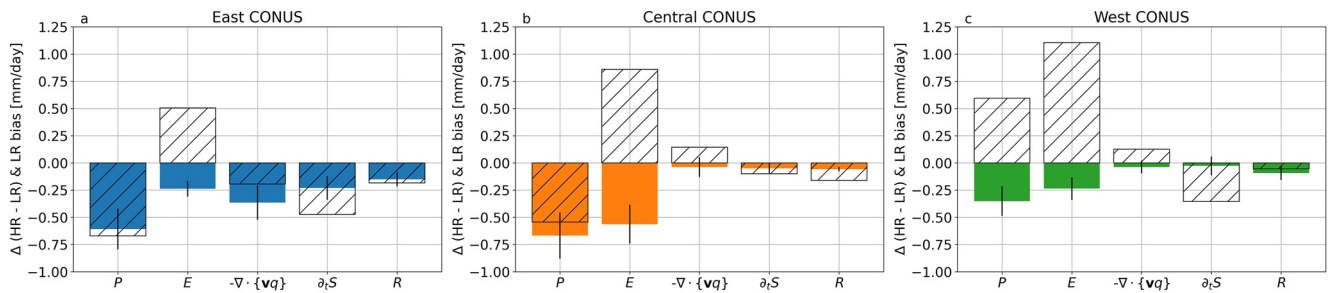


Figure 11. Mean difference between LR and HR (colored bars), and mean bias for LR (hatched bars) for precipitation, ET, atmospheric moisture convergence, terrestrial water storage tendency, and runoff for (a) Eastern CONUS, (b) Central CONUS, and (c) Western CONUS. The error bars provide the 95% confidence interval for the mean differences. All values have units of mm/day.

For atmospheric moisture convergence, the change from LR to HR is largest over the Eastern CONUS. The reduction in moisture convergence is consistent with a divergent circulation experiencing an increase in atmospheric moisture, but the panel I of Figure 10 does not vary as smoothly as Figure S7a in Supporting Information S1, suggesting a role for a dynamical response as well. While we leave a full exploration of the circulation response to future work, there is a notable change in the North American Subtropical High (NASH), which primarily impacts the Eastern CONUS. Figure S8 in Supporting Information S1 shows a westward expansion of the NASH with increased resolution. Future work is needed to fully understand the role of changes in the NASH and the moisture convergence over the Eastern CONUS in E3SM. There is no statistically significant change in moisture convergence over the Central or Western CONUS regions. Terrestrial water storage anomaly shows the largest differences over steep terrain in the Western CONUS, with some smaller changes of either sign occurring elsewhere. Similarly, runoff shows the largest changes over terrain in the Western CONUS, but also shows decreases in value in HR relative to LR over the Eastern CONUS.

As already demonstrated with the stoplight diagrams, these changes do not always manifest as decreases in the bias. The center two columns of Figure 10 visually confirm that finding. The reduction in precipitation over the Western CONUS, the reduction in ET over the Eastern and Western CONUS, and the reduction in runoff over the Western CONUS are where we see significant improvements from increasing resolution relative to the reference set.

We can reduce statistical uncertainty by grouping months into seasons and the watersheds into the three regions shown in Figure 1: the Eastern CONUS (watersheds 1–6), the Central CONUS (watersheds 7–12), and the Western CONUS (watersheds 13–18). We perform this grouping to better understand how the water cycle budget term changes relate to one another. We continue to focus on the warm season (JJA).

Figure 11 shows the changes in each metric averaged over each region (in the colored bars), as well as the LR bias (hatched bars). Where the bars have opposite signs shows a reduction in the bias going from LR to HR. Across all three regions, this only happens for ET. Figure 11 shows that ET improves over the Central CONUS, while Figure 6 shows little improvement. As can be seen from Figure S2 in Supporting Information S1, this results from large uncertainties between observational products during the warm season. The MODIS ET product used in Figures 10 and 11 tends to have lower values than the GLEAM and DOLCE products over the Central CONUS (Figure S2 in Supporting Information S1), making the LR bias larger.

Atmospheric moisture convergence shows a bias reduction for both the Central and Western CONUS, while precipitation only shows improvement over the Western CONUS (in agreement with the stoplight and map plots shown earlier). To make the units consistent, we show the time-tendency of the terrestrial water storage anomaly. The biases are exacerbated for this term over the Eastern and Central CONUS, with no significant change over the Western CONUS. Runoff is worse over all three regions at HR compared to LR. The overall slowdown of the water cycle is readily apparent in Figure 11. Every single difference term is negative or statistically indistinguishable from zero.

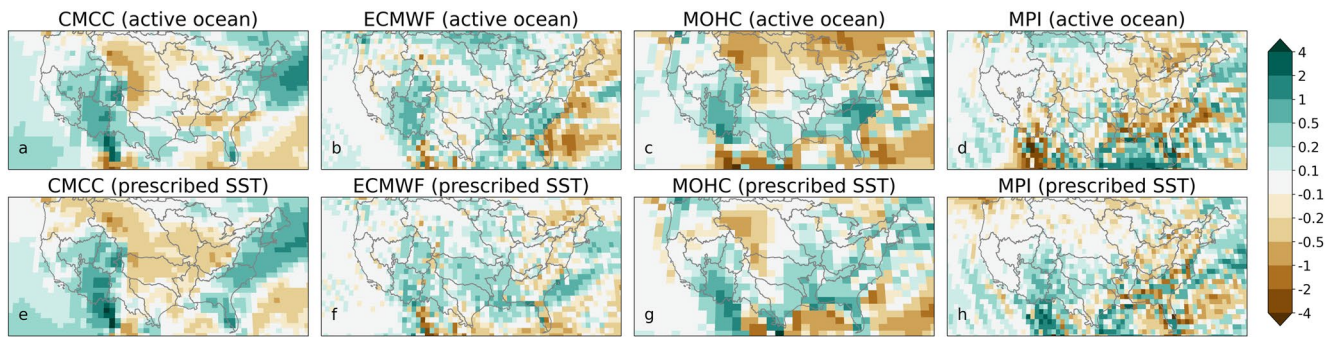


Figure 12. JJA mean precipitation change (HR minus LR) for a selection of other HighResMIP models. (a–d) Simulations with an active ocean model. (e–h) Simulations with prescribed SSTs. All values have units of mm/day.

4.3. Local Versus Remote Influences of Resolution Change

All of the analyses so far are diagnostic in nature. A conclusive explanation for the drying of the land and slow-down of the water cycle is difficult to attribute to local resolution impacts in these coupled simulations. As shown in Figure 4, the HR simulation is much warmer than the LR simulation. It is possible that this global temperature signal may play a role on top of the local effects of grid refinement, potentially through changing equator-to-pole gradients (see the bottom panel of Figure 4). There is evidence that decreasing equator-to-pole temperature gradients lead to decreases in mid-latitude terrestrial precipitation (e.g., Routson et al., 2019), though testing that specific hypothesis is beyond the scope of the current work. While it is worth noting that there is no widespread reduction in precipitation and ET across the watersheds from warming in the abrupt quadrupling of CO₂ experiment in E3SMv1 at low-resolution (Figure S9 in Supporting Information S1), this fact alone does not rule out the role of remote SST changes on the water cycle differences between HR and LR observed here.

It is tempting to envision running the LR simulation with SSTs prescribed from the HR simulation to quantify the impact of remote SSTs on the CONUS water cycle changes. Under such a scenario, the global mean temperature would be similar, despite land temperatures being able to vary between the two experiments. Such an experiment, however, removes the two-way interactions between the atmosphere and ocean. This coupling is important to regional water cycle features. For example, Harrop et al. (2019) did exactly the above experiment where the SSTs from a coupled E3SMv1 simulation (the abrupt quadrupling of CO₂ experiment) were used to run a prescribed SST experiment. They found noticeable differences over the South Asian Monsoon between the two experiments, despite their shared SST patterns. Using their simulation output, we find that the changes in precipitation going from interactive to prescribed SSTs over the CONUS exceed those going from LR to HR (Figure S10 in Supporting Information S1). Therefore, such an experiment may not be well suited for quantifying how much of the water cycle change comes from improved local resolution and how much comes from global scale sensitivity to resolution. It could, however, also be that the monthly data used to prescribe the SSTs miss important shorter timescales that are necessary to represent the surface-air coupling. Disentangling such an effect is beyond the scope of this work, and we leave it to future research efforts.

An alternative option that has greater appeal involves running E3SM with a regionally refined mesh, where the high resolution region is constrained to a small region of interest (e.g., the CONUS), and the remainder of the globe uses the low resolution grid spacing. Such a configuration could allow for simulations to be compared where the global values (such as surface temperature) remain similar. A regionally refined mesh was used with E3SMv1, but global means are not the same between the regionally refined version and the uniform low-resolution owing to differences in model parameter values (Tang et al., 2019). The North American regionally refined mesh used for E3SMv2 has the same parameter values as the E3SMv2 uniform low-resolution mesh and their global temperature values are similar (Tang et al., 2022). Similar analyses of the water cycle metrics presented here will likely be valuable for those simulations.

To add context to the precipitation responses, Figure 12 shows precipitation responses (HR minus LR) for a selection of other HighResMIP models using active ocean (top row) and prescribed SSTs (bottom row). Details on the other HighResMIP models used are provided in Table 4. There is little consistency across these models in the precipitation response to resolution, and none of these models show the same uniform decrease in precipitation

Table 4
Simulation Details for the Selection of Other HighResMIP Models Used

Model name	Institution	HR grid	LR grid	Reference
CMCC-CM2	CMCC	1,152 × 768	288 × 192	Cherchi et al. (2019)
ECMWF-IFS	ECMWF	720 × 361	360 × 181	C. D. Roberts et al. (2018)
HadGEM3-GC3.1	MOHC	1,024 × 768	192 × 144	M. J. Roberts et al. (2019)
MPI-ESM1-2	MPI	768 × 384	384 × 192	Gutjahr et al. (2019)

that E3SM shows. Like E3SM, the CMCC, MOHC, and MPI models exhibit the strongest decreases in precipitation with increasing resolution over the Eastern and Central regions of CONUS. Unlike E3SM, however, none of the models show a decrease in precipitation with increasing resolution over the Western CONUS. The agreement in precipitation change is modest between the active ocean and prescribed SST experiments, suggesting SST patterns may play only a minor role in determining CONUS water cycle changes. The disagreement between the models suggests future research is still needed to understand the specific pathways by which each of these models' water cycle changes manifest.

5. Additional Metrics

It is worth examining several other metrics that we anticipate to be sensitive to resolution. These include measures of the precipitation distribution and its relation to storm systems, snowpack, and streamflow. These metrics will be covered in the following subsections. In particular, we expect certain storm features responsible for extreme precipitation to exhibit precipitation production that matches observations closer in HR than LR. These systems include TCs, ETCs, and ARs.

5.1. Precipitation Distribution and Its Relation to Storm Events

To better understand the water cycle changes with resolution, we begin by examining a simple measure of the precipitation distribution for each watershed. The metric we use is the unevenness, designed by Pendergrass and Knutti (2018) to quantify the contribution of heavy rainfall days to the total annual amount. Unevenness is defined as the number of days required to reach 50% of the total annual rainfall. It is computed by sorting the daily rainfall from most to least precipitation. The data is then cumulatively summed, divided by the total annual rainfall, and the unevenness value is the value of the sequence equal to 0.5 (computed by linear interpolation). It is important to note that smaller values of this parameter mean that precipitation is more “uneven.”

Pendergrass and Knutti (2018) found that the wettest 12 days account for half of the annual precipitation in observations (a collection of surface observing stations and TRMM data). Models, on the other hand, tend to have much less unevenness, requiring roughly twice as many days as observed to reach 50% of their annual total precipitation. Part of the bias is a result of too frequent light rain in models (Stephens et al., 2010), which is true of E3SM as well (Terai et al., 2017). Caldwell et al. (2019) showed an increase with increasing resolution in the heaviest rain rates over tropical regions in E3SM and we hypothesize that similar increases (and hence improvements in unevenness) will be detectable over the CONUS.

Table 5 shows the unevenness metric for the HR and LR experiments, as well as TRMM data. The unevenness is smaller for HR than LR, meaning it takes fewer days to accumulate 50% of the annual precipitation when the HR grid is used. The improvement in a shift toward higher rain rates with increasing resolution has been noted previously, but is not always the case (L. Zhang et al., 2016), so it is encouraging to see this response from E3SM. Because the unevenness is normalized by the total rainfall in its definition, an increase in unevenness (fewer days to reach half of the year's total) implies a shift in the rain fall distribution toward higher rain rates, regardless of the sign of the mean change. While the values presented in Table 5 are those computed on the native grid of each data source, Pendergrass and Knutti (2018) showed that the unevenness metric is sensitive to regridding (with larger values for coarser grid spacing). Thus for determining whether the differences in unevenness are statistically significant between LR and HR, the HR data were regridded to the LR mesh for

Table 5
Unevenness for Tropical Rainfall Measuring Mission, E3SM HR, and E3SM LR

Watershed	01	02	03	04	05	06	07	08	09	10	11	12	13	14	15	16	17	18
TRMM	14	14	15	12	15	16	12	13	–	13	11	9	9	15	9	12	–	8
E3SM HR	27	25	24	27	27	25	21	20	23	25	18	16	19	29	15	26	35	15
E3SM LR	30	29	30	33	33	32	27	26	26	31	25	21	24	40	20	34	43	19

Note. Values provided in the table are all for the native grid of the data. The TRMM data are omitted for watersheds 9 and 17 owing to part of that watershed occurring outside of the TRMM data boundaries.

significance testing. All watersheds show a statistically significant difference in unevenness between LR and HR, even when both data are on the same mesh. The regridding effect increases the unevenness metric by about 1.5–4.5 days (not shown). The increase in the value of unevenness owing to regridding is smaller than the increase when comparing the LR experiment to the HR experiment. The TRMM data show that even at HR, E3SM still significantly overestimates the unevenness metric, meaning total precipitation is still too uniformly spread across days of the year.

The Upper Colorado (14) watershed shows the largest unevenness sensitivity to resolution, with large changes also present in the Great Basin (16), Pacific Northwest (17), Arkansas-White-Red (11), Tennessee (6), and Missouri (10) watersheds—all exceeding a 6-day mean increase in unevenness. The Western CONUS tends to see larger unevenness sensitivity to model resolution than the Eastern or Central CONUS regions, suggesting better-resolved topography at HR improves the distribution of precipitation rates for these watersheds. The average bias in unevenness for the watersheds (not including the Souris-Red-Rainy (9) and Pacific Northwest (17) watersheds) is 17.6 days for the LR simulation and 12.3 days for the HR simulation. These biases are comparable to the biases in the CMIP5 archive relative to station data (Pendergrass & Knutti, 2018).

The GPCP 1 degree daily (1DD) product was also examined for comparison with the HR and LR simulations, but is not shown owing to a switch in data processing within that product at 40°N that complicates the interpretation of the northern watersheds. The GPCP 1DD uses the Threshold-Matched Precipitation Index between (40°S–40°N) and switches to scaling with Television and Infrared Observation Satellite Operational Vertical Sounder (TOVS; Huffman et al., 2001) at higher latitudes. This switch in how rainfall is determined for the GPCP 1DD product significantly impacts the unevenness metric (not shown), though the switch is not discernible in other features such as monthly mean precipitation.

The unevenness results suggest stronger rainfall events occur for E3SM HR compared to LR. It is worth asking if similar changes can be observed in the precipitation extremes. To evaluate the simulation of seasonal precipitation extremes in the HR and LR experiments, we use generalized extreme value (GEV) distributions to model extremes of daily precipitation and compute the return levels associated with a 20-year extreme event. We use a block (seasonal) maxima approach, where we estimate a GEV distribution of the maxima of a block of data. Here, the block size is a season. We first aggregate daily aggregated precipitation over the watershed basin scales. The seasonal maxima of daily precipitation are computed for each watershed for each year. A GEV distribution is then estimated at each watershed using the seasonal maxima data (sample size of 20 for GPCP data, and 30 for HR and LR runs) using the maximum likelihood method. A GEV distribution, $G(z)$, of block maxima, z , has three parameters - location (μ), scale (σ) and shape (ξ) - and is represented as follows for $\xi \neq 0$:

$$G(z) = \exp \left\{ - \left[1 + \xi \left(\frac{z - \mu}{\sigma} \right) \right]^{-1/\xi} \right\} \quad (3)$$

$G(z)$ is computed as the limit of the equation as $\xi \rightarrow 0$, if $\xi = 0$ (Coles, 2001). These parameters are approximately multivariate normal, and the associated variance-covariance matrix is computed at the maximum likelihood estimates. We also conduct a Kolmogorov-Smirnov goodness of fit test to evaluate the null hypothesis that the empirical distribution is statistically equivalent to the derived GEV distribution at the 95% confidence level. We find that the null hypothesis is accepted for all GEV estimates. The return level of a τ -year event can be computed by inverting the model as follows (when $\xi \neq 0$):

$$R(\tau) = \mu + \frac{\sigma}{\xi} \left(-\log(1 - 1/\tau)^{-\xi} - 1 \right) \quad (4)$$

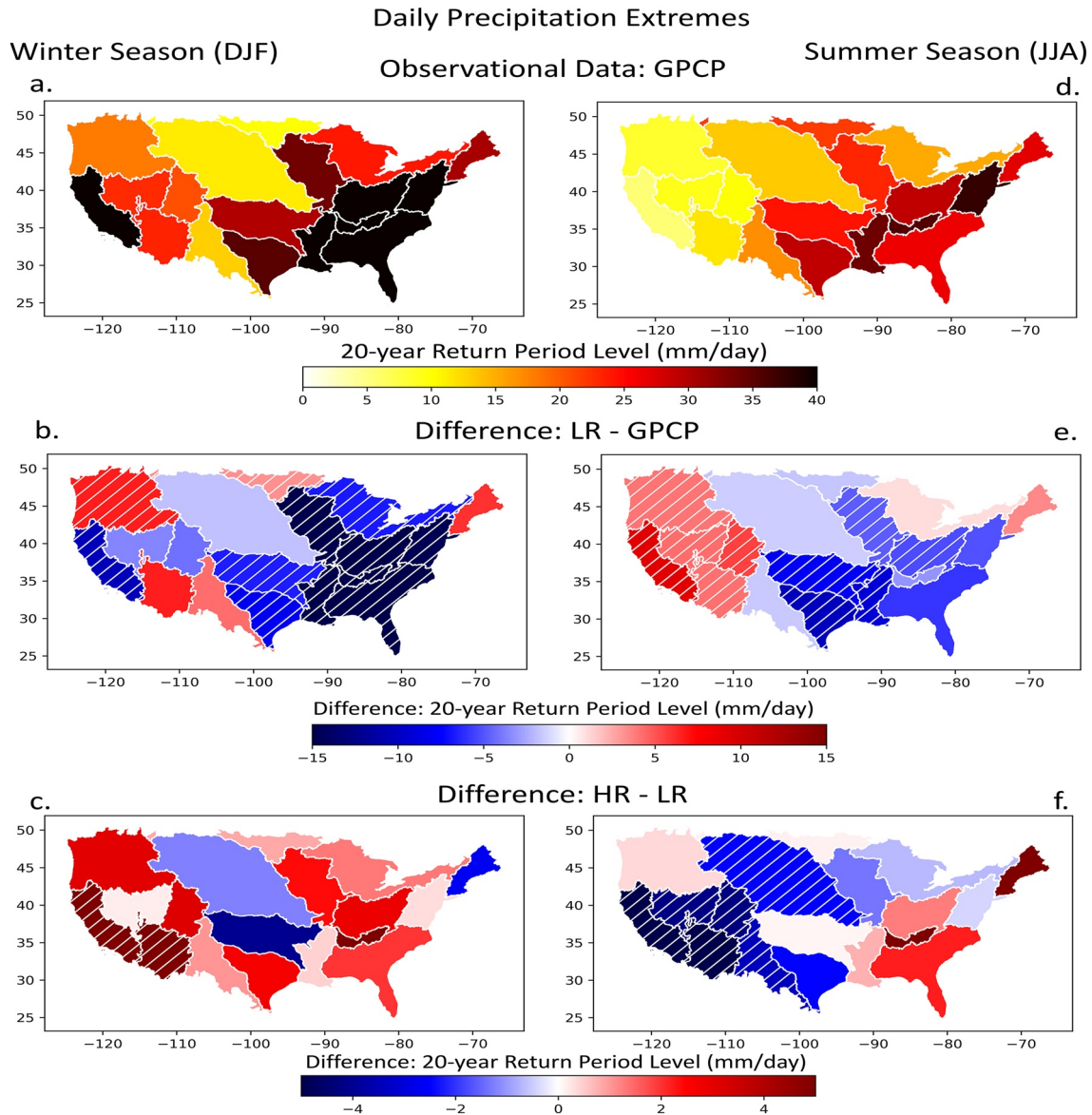


Figure 13. Return levels of 20-year extreme events. Return levels of 20-year extremes of daily precipitation aggregated over Hydrologic Unit Codes watershed scales for Global Precipitation Climatology Project (GPCP) precipitation data during (a) winter and (d) summer season. Difference between (b, e) LR and GPCP and between (c, f) HR and LR for winter and summer season. Hatching in (b), (c), (e), (f) indicates watersheds where the difference in return levels are statistically different from zero at the 95% confidence level.

and its limit when $\xi = 0$ (Coles, 2001). The variance-covariance matrix of the GEV parameters can also be used to compute the associated standard errors of $R(\tau)$, and we use these standard errors here to conduct statistical tests.

Figure 13 shows the return level of a 20-year extreme event for GPCP for the winter and summer seasons for all the HUC2 watersheds. Somewhat surprisingly, the switch in rainfall calculation poleward of 40° for GPCP described above has virtually no impact on the GEV calculation for extremes described below (not shown). An exact explanation for why unevenness is more sensitive to the change in GPCP rainfall than the extremes is beyond the scope of this manuscript. The pattern of extreme precipitation over the CONUS is similar to other measures of extreme rainfall previously reported (Akinsanola et al., 2020). Also shown are the differences between LR and GPCP. Hatchings indicate watersheds where the difference is statistically significant at the 95% confidence level based on a two-tailed Student's t -test. The LR shows a strong, statistically significant negative bias over watersheds in the eastern half of the CONUS, simulating weaker than observed extremes in both the winter and summer seasons. The model also exhibits a negative bias over California (18) and a positive bias over

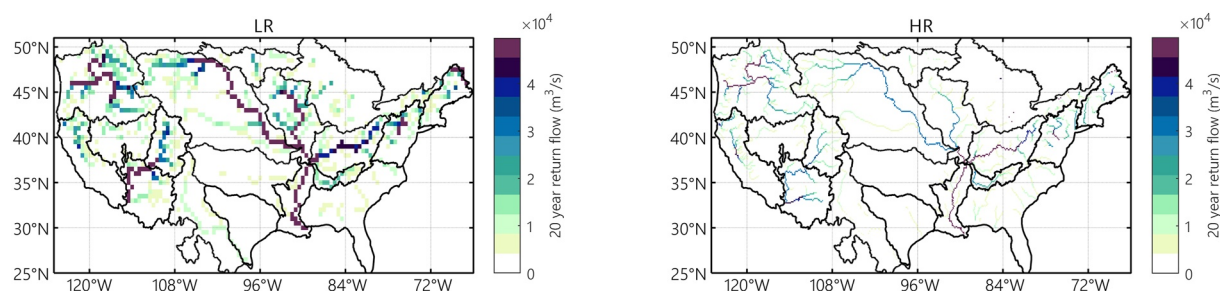


Figure 14. Twenty year return flow for river discharge over CONUS for the LR (left) and HR (right) experiments. Units are m^3/s .

the Pacific Northwest (17) in the winter season. Over the western watersheds the model shows a positive bias in the summer simulating stronger than observed extremes, which are statistically significant. This is consistent with simulations with other models at similar resolutions which generally underestimate precipitation extremes over the Southeast CONUS and overestimate it over Western US (Srivastava et al., 2020).

Figure 13 panels c and f show the difference between the HR and LR simulations for the winter and summer seasons. The HR experiment simulates stronger extremes than the LR experiment over the Eastern CONUS, generally reducing the bias there. However, the improvements are not statistically significant. Over California (18), HR produces stronger extremes than LR, which are statistically significant, reducing the bias there. Wintertime extremes over the Western CONUS are larger at HR than LR, though California (18) and the Lower Colorado (15) are the only significant differences.

While warm-season precipitation is reduced in HR relative to LR across all of the CONUS, as seen in Sections 4.1 and 4.2, the precipitation extremes do not behave uniformly. During the summer season, the changes in simulated extremes between HR and LR are the opposite of winter, with HR producing less intense extreme summertime precipitation events over all watersheds except the Pacific Northwest (17), reducing much of the biases between LR and GPCP. Despite the differences not being statistically significant, similar improvements are hinted at for the Southeast CONUS, consistent with previous grid-point based studies (Mahajan et al., 2015; M. F. Wehner et al., 2010, 2014).

Extreme precipitation can lead to extremes in river discharge. Rivers transport the runoff from the land to the ocean through river channels. Streamflow is the flow discharge rate in the river, which is of particular importance to society in terms of water supply for municipal and agriculture purposes, transportation, and hydropower generation and environmental flows. On the other hand, extreme streamflow events, or floods, are one of the most frequent

types of natural disasters created by rivers. In this study, we examine flood events between LR and HR by comparing the 20-year streamflow extreme events over the HUC2 regions using the same GEV distribution method used to examine extreme precipitation (Equation 3). For each gridcell, maximum daily streamflow discharge for each year was computed and fit with the GEV distribution. The MOSART river model uses latitude-longitude grids for river modeling, with 0.5 degree for LR and 0.125 degree for HR. Since streamflow distribution is intrinsically tied to the river network, it is more reasonable to investigate it at the model native grid resolutions.

Figure 14 shows maps of extreme streamflow over the CONUS. Visual comparison between LR and HR in Figure 14 shows larger values of extreme streamflow are more common in the LR configuration. Examining the cumulative distribution function of the 20 year return flow (Figure 15) confirms this feature. These results suggest that the general decrease in runoff seen across the CONUS leads to a general decrease in streamflow extreme intensity. For individual watersheds, there is considerable variability in whether more intense streamflow extremes are found at LR or at HR (see Figures S11–S28 in Supporting Information S1), despite runoff generally decreasing with increasing resolution across the CONUS. These results suggest that the physical characteristics of the river channel may be a larger factor

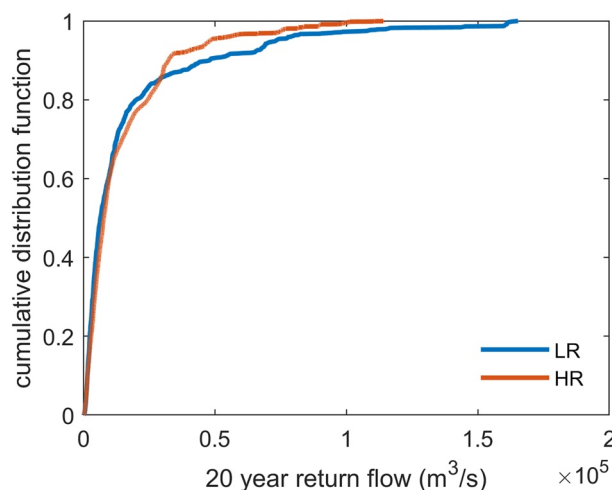


Figure 15. Cumulative distribution of 20 year return flow for river discharge over continental United States for the LR (blue) and HR (orange) experiments. Units are m^3/s .

Table 6
Criteria for Classifying Precipitation Associated With Particular Features

Feature	Criteria
TCs	Precipitation within 5° great-circle-distance of a TC point
ARs	Precipitation clusters >40 mm/6 hr which are connected to detected AR features, unless already classified as TC precipitation
ETCs	Precipitation within 10° great-circle-distance of a ETC point, unless already classified as TC or AR precipitation

in determining streamflow extremes across these resolutions than the changes in runoff. One exception appears to be the California (18) watershed, which is the one watershed with an increase in runoff at HR relative to LR, and also sees a significant increase in extreme streamflow at HR relative to LR (see Figure S28 in Supporting Information S1).

5.2. Feature Based Precipitation

To better understand the upstream atmospheric features responsible for precipitation, we employ Tempes-Extremes (Ullrich et al., 2021) to track TCs, ARs, and ETCs, as described in Appendix A. The catalogs of tracked features are then used to extract precipitation associated with each of these features following the criteria given in Table 6. While precipitation could be due to multiple features, in this analysis we associate precipitation first with TCs, then with ARs, then with ETCs, in order; as ARs and ETCs are often not distinct features, here ETC precipitation refers to ETC-related precipitation that is not already associated with an AR. Figure 16 shows total annual precipitation from LR, HR, and ERA5 reanalysis, and the percentage contribution associated with the occurrence of these three feature types. ERA5 is used here for both feature tracking and precipitation because it provides precipitation that is coincident in time with the features being tracked. In other words, the precipitation fields are consistent with the reanalysis circulation patterns that are being tracked.

Figure 16 shows improvements in the contribution to precipitation from the tracked features. TCs, in particular, show significant improvement at HR compared to LR which has been examined in detail by Balaguru et al. (2020). ETCs show improvement as well, though the changes are somewhat modest relative to the biases.

Table 7 shows the regional contributions of each feature type, as well as a residual category—the precipitation contribution not associated with TCs, ARs, or ETCs. The residual category shows a decline in percentage contribution to the total over each region when comparing HR to LR. This decline in precipitation not associated with large-scale forcing from TCs, ARs, or ETCs brings the model closer to ERA5 over the Eastern and Central CONUS regions, but farther from ERA5 over the Western CONUS. Consistent increases across regions occur for both TC and AR contributions to precipitation (consistent with earlier findings by Chang et al. (2020)). The bias in AR contributions is particularly large for the Western CONUS. This is not surprising since it has been previously noted that a similar model, the CESM, has been shown to have ARs that are too strong and last too long during landfall at ~25 km resolution (Rhoades et al., 2020a, 2020b, 2021).

We use the Shannon Diversity Index (SDI) normalized by the natural log of the number of weather types present to quantify how similar the populations of weather types are between the LR, HR, and ERA5. We set a minimum percentage of 0.1% to have a weather type be considered present. The normalized SDI is computed as

$$SDI = \frac{-\sum_{i=1}^N p_i \ln(p_i)}{\ln(N)} \quad (5)$$

where p_i is the proportion of total precipitation for weather type i (including the residual category), and N is the total number of categories. The normalized SDI is provided in the last row of Table 7. In the Eastern and Central regions, the HR population becomes closer to that of the ERA5, and the normalized SDI is closer to 1 (a more diverse population). In the Western CONUS, the SDI is farther from ERA5, though still closer to 1 at HR compared to LR. These results are consistent with the general trend of HR producing a larger fraction of its total precipitation from TCs, ARs, and ETCs.

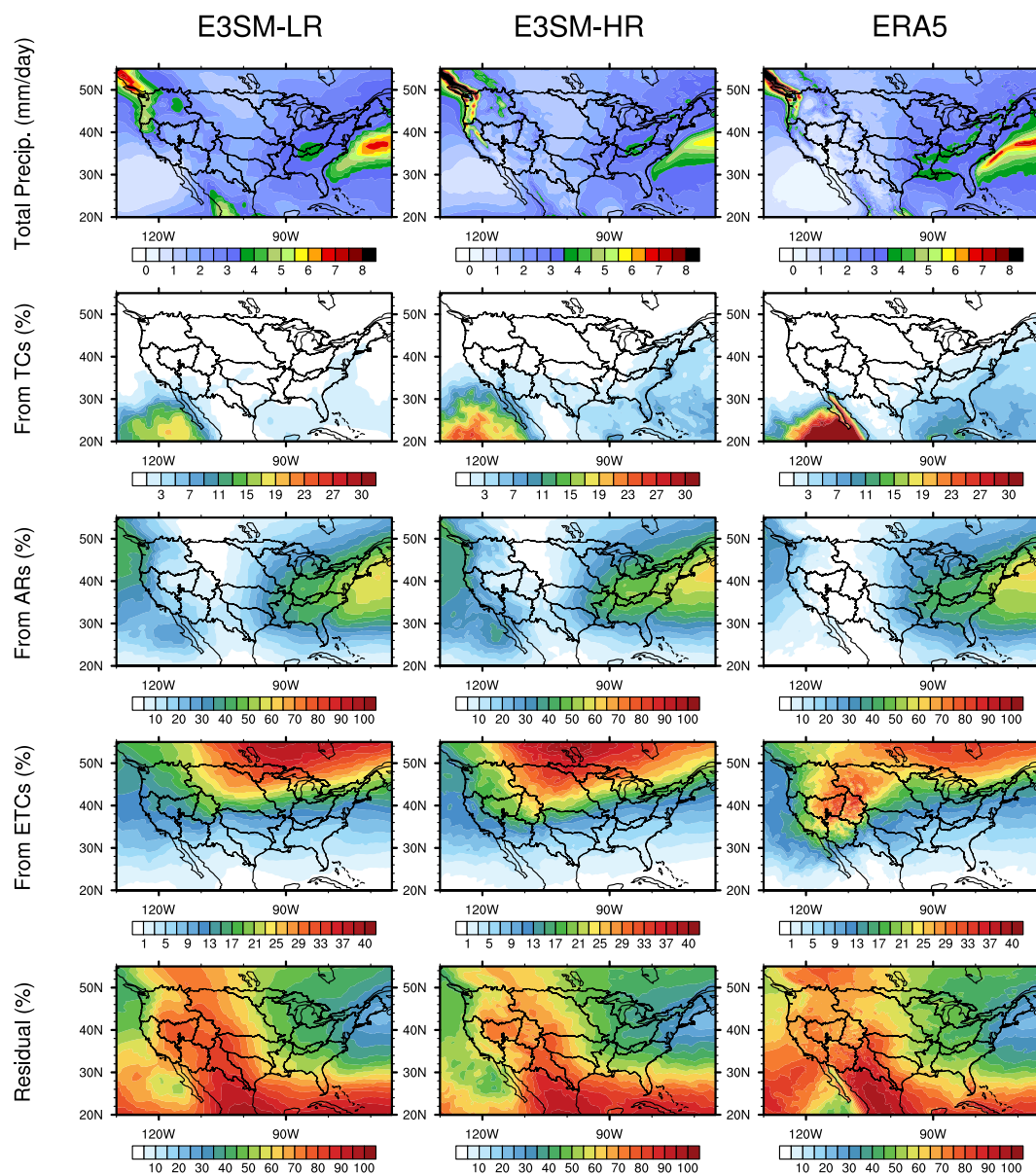


Figure 16. Total annual precipitation from E3SM-LR, E3SM-HR, and ERA5 (in mm/day), and fractional contribution of precipitation associated with three tracked feature types: tropical cyclones, atmospheric rivers, extratropical cyclones, and residual precipitation.

Table 7
Annual Mean Percentage Contribution to Precipitation Totals in Each Conterminous United States (CONUS) Region, Filtered by Associated Features

HUC2 region	Eastern CONUS			Central CONUS			Western CONUS		
	LR	HR	ERA5	LR	HR	ERA5	LR	HR	ERA5
Tropical Cyclones	0.6%	2.3%	2.2%	0.4%	0.7%	0.7%	0.4%	0.8%	0.2%
Atmospheric Rivers	42.8%	44.7%	41.1%	20.8%	23.4%	25.2%	17.6%	19.9%	10.1%
Extratropical Cyclones	13.2%	11.6%	11.6%	15.9%	17.3%	14.9%	13.3%	16.4%	20.1%
Residual	43.4%	41.5%	45.2%	62.9%	58.5%	59.2%	68.8%	62.9%	69.6%
Normalized SDI	0.74	0.77	0.76	0.67	0.72	0.70	0.61	0.68	0.59

We have also examined the time period of greatest precipitation change between LR and HR examined in Sections 4.1 and 4.2 (JJAS for the Eastern and Central CONUS and AMJJ for the Western CONUS). The results are tabulated in Table S1 in Supporting Information S1. Since the large-scale forcing tends to be weaker in the warm season, the fraction of precipitation coming from ARs and ETCs is significantly lower during the warm months. There are increases in TC precipitation fraction for the Eastern and Central CONUS, while there is no TC precipitation over the Western CONUS (which is not surprising given the season). In all three regions, the normalized SDI shows that the HR population becomes closer to that of the ERA5 relative to LR, and the normalized SDI is closer to 1 (a more diverse population). These results suggest that HR does make modest improvements to simulated storm features, regardless of the sign of the mean bias change. It is important to caution that the reapportionment of precipitation across events is not necessarily the cause or effect of the total precipitation decline. Future studies will be needed to better understand the connections between the simulated storms and the total precipitation.

5.3. Snowpack

The final metric investigated for this study is mountain snowpack. Mountain snowpack is a key natural reservoir of water in the mountainous western United States (Livneh & Badger, 2020; Lynn et al., 2020; Mote et al., 2018; Siirila-Woodburn et al., 2021; Sturm et al., 2017), often shown through snow water equivalent (SWE). From a modeling perspective, SWE also provides a unique litmus test in validating a model's ability to represent cross-scale, spatiotemporal interactions between precipitation, radiation, and temperature over the water year (He et al., 2019; Krinner et al., 2018; McCrary et al., 2017; Xu et al., 2019), with important feedbacks to other components of the mountainous hydrologic cycle (e.g., soil moisture, runoff, and groundwater recharge). To validate a model's ability to represent the seasonal snow cycle over a given water year, Rhoades et al. (2018a, 2018b) developed a multi-metric framework known as the SWE triangle that built off work of Trujillo and Molotch (2014). This model benchmarking framework represents a linear decomposition of the seasonal snow cycle (which resembles a triangle) and includes metrics such as the snow accumulation and snowmelt rate (sides), the accumulation, melt, and snow season length (base), and the peak SWE volume and date of peak SWE, or peak accumulation date (vertex). The SWE triangle multi-metric framework was also developed with resource manager input, or what have been referred to as use-inspired metrics (Jagannathan et al., 2020). As such, peak SWE volumes are communicated in million-acre feet (MAF), or the amount of water needed to flood an acre sized field by one-foot, which is commonly used terminology in water resource management in the United States.

Figure S29 panels a and b in Supporting Information S1 present two examples, a continental (Upper Colorado, 14) and a maritime (California, 18) mountain range, of seasonal snowpacks simulated over the 30-year historical period by the HR and LR experiments decomposed using the SWE triangle framework and compared with ERA5. These two mountain ranges are sub-selected from the five shown in Figure 17 as they represent two of the largest relative changes in snow cycle representation with resolution between LR and HR. Interestingly, seasonal snowpacks in the Upper Colorado (14) and California (18) watersheds have opposite responses in E3SMv1 to a four-times refinement of horizontal resolution. In the Upper Colorado (14), climatological average peak SWE volumes are smaller in HR than LR (31 ± 3 MAF and 37 ± 4 MAF). Although peak SWE timing is comparable between LR and HR, and overlaps with ERA5 (9 March), the reduction in peak SWE in HR, though still too high, more aligns with ERA5 (19 ± 2 MAF). Conversely, in the California (18) basin, peak SWE volumes increase by 6 MAF from LR to HR (7 ± 2 MAF to 13 ± 2 MAF), which is more comparable to ERA5 peak SWE estimates (15 ± 2 MAF) and another observation-based gridded SWE product (16 ± 3 MAF) produced by Margulis et al. (2016) for water years 1985–2015. Peak SWE timing is also enhanced in HR relative to LR and when compared with ERA5. The complete suite of SWE triangle metrics for both the California (18) and the Upper Colorado (14) watersheds, as well as the three other mountain watersheds of the western United States, are depicted in Figure 17.

Notably, the increase in SWE in the California (18) and Pacific Northwest (17) regions occurs despite a decrease in annual total precipitation owing to a larger fraction of that total precipitation falling as snowfall instead of rain in the HR experiment (Figure S30 in Supporting Information S1). Figure S30 in Supporting Information S1 shows that the increase in snowfall fraction is concentrated over the Cascade and Sierra Nevada mountain ranges. The changes in snow fraction are anti-correlated with 2 m air temperature ($r = -0.86$). Most of the CONUS experiences warming consistent with the warming SSTs, but over regions of complex topography, the increase in

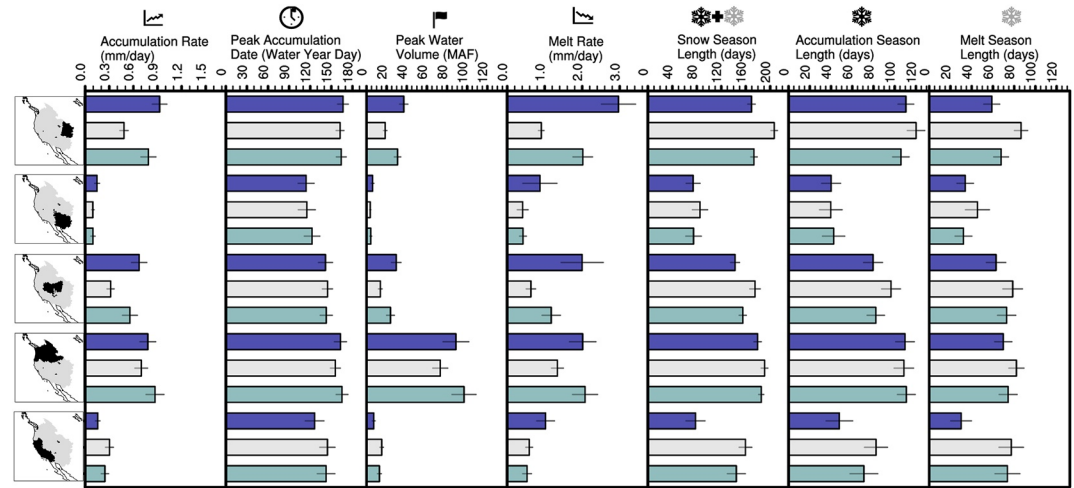


Figure 17. The seasonal snow cycle is characterized by its daily snow water equivalent (SWE) and linearly decomposed using the SWE triangle methodology to assess the western United States mountainous hydrologic units for the E3SM low-resolution (LR, 1.00°, blue) and high-resolution (HR, 0.25°, aquamarine) simulations spanning 1985–2014 (see Figure S29 in Supporting Information S1 for examples of two individual watersheds). ERA5 is shown in gray. The bars indicate the 30-year climatological average conditions simulated across all five mountainous hydrologic units of the western United States (in order of appearance in each row from top to bottom, Upper Colorado, Lower Colorado, Great Basin, Pacific Northwest, and California) for each of the seven SWE triangle metrics (columns and histograms) with 95% confidence intervals indicated (black lines).

horizontal resolution allows for colder temperatures at higher elevations, also seen over the Cascade and Sierra Nevada mountain ranges (not shown).

6. Discussion and Summary

In this manuscript, we have examined the resolution sensitivity of the seasonal water cycle over the CONUS at the HUC2 watershed scale using E3SMv1 simulations run at low and high resolution. The results show a slow down of the warm season water cycle with increasing resolution, with decreases in precipitation, evapotranspiration, moisture convergence, terrestrial water storage anomaly tendency, and runoff. The largest differences happen during JJAS for the Eastern and Central CONUS, and AMJJ for the Western CONUS. Whether the decreases in these terms result in reductions in biases or not depend on the region and the budget term. Precipitation, for example, shows worsening biases with HR over the Eastern and Central CONUS, but reductions in biases over the Western CONUS. ET, on the other hand, shows reduced biases with HR over all three CONUS regions. These differences highlight some of the difficulty in correcting biases in models like E3SM, since reductions in precipitation and ET improve one while worsening the other.

The warm season slowdown of the water cycle over the CONUS is not present over all land regions in E3SM. Similarly, the broad precipitation decrease pattern over CONUS when increasing resolution in E3SM is not seen in several other HighResMIP simulations. It is worth noting that there is not much agreement on the precipitation response to increasing resolution among those other HighResMIP models. Future sensitivity experiments and additional analyses will be needed to determine the exact mechanisms responsible for the slowdown of the water cycle with resolution in E3SM.

Inspired by the suggestions of Pendergrass et al. (2020), we examined additional metrics involving precipitation distributions, extreme precipitation and streamflow, storm feature contributions to precipitation, and snowpack to further assess the simulated water cycle in E3SMv1 at both low and high resolution. The HR experiment generates days with more intense precipitation, leading to reduced values of unevenness across all watersheds. Extreme precipitation, as measured by the 20-year return period level, shows both increases and decreases depending on season and watershed. Generally, however, the changes in extreme precipitation act to reduce biases in the LR experiment relative to observed precipitation extremes. Similarly, extreme streamflow also shows a lot of watershed to watershed variability in its response to increasing horizontal grid spacing. The HR experiment generally

shows modest improvements in the distribution of tracked storms: TCs, ARs, and ETCs. Finally, the snowpack metrics show better agreement with ERA5 and observations over many of the Western CONUS watersheds at HR relative to LR. Taken all together, these results suggest that the HR experiment is doing a better job at reproducing the physical processes that occur within the water cycle, but the mean biases in exchanges of water between the land and atmosphere, as well as their lateral transports, still remain a challenge.

We have discussed potential future work to help isolate the role of local grid refinement relative to remote changes in climate state such as SST patterns. Our results have shown that the global mean temperature increase in HR relative to LR is insufficient to explain the water cycle slow down, since it is not reproduced in other E3SMv1 warming experiments. Additionally, the ocean-atmosphere coupling is too important to the simulated water cycle to allow for prescribing the SST patterns from the HR at LR. Regional refinement is an exciting experimental design that may help discern the local and remote influences of grid refinement on the simulated CONUS water cycle. The regionally refined E3SMv2 experiments will need to be examined in future work to help disentangle this particular issue. Additionally, this work highlights the need for more ensemble members. Changes in the moisture convergence and terrestrial water storage anomaly tendency terms were only statistically discernible when aggregated over regions and seasons, but it is possible that with an ensemble of simulations, such differences could be quantified at the watershed and monthly scales.

While this study highlights many important sensitivities of the water cycle to model resolution, one aspect that is not covered is how resolution might change the sensitivity of the water cycle to climate change. More work is needed to understand what, if any, impacts increased horizontal resolution in E3SM has on the water cycle response to transient warming. Given its importance to society, continued effort is needed for understanding how earth system models like E3SM represent the water cycle and its sensitivity to changes within those models.

Appendix A: Feature Tracking With TempestExtremes

Command line arguments for TempestExtremes (TE) are described in the TE user guide (Ullrich, 2021). Tracking with TE is performed on the native E3SM grid (ne30 or ne120). For identifying tropical cyclones (TCs) we use the following TE commands (excluding input/output data arguments for brevity):

```
DetectNodes
--searchbymin PSL
--closedcontourcmd "PSL,200.0,5.5,0;_DIFF(Z200,Z500),-6.0,6.5,1.0"
--mergedist 6.0
--outputcmd "PSL,min,0;U10,max,2;_DIV(PHIS,9.81),min,0"

StitchNodes
--in_fmt "lon,lat,slp,wind,zs"
--range 8.0
--mintime "10"
--maxgap "3"
--threshold "wind,>=,10.0,10;lat,<=,50.0,10;lat,>=,-50.0,10;zs,<=,15.0,10"
```

PSL is the pressure at sea-level, Z200 and Z500 are the geopotential height at 200 hPa and 500 hPa, respectively, U10 is the 10 m wind speed, and PHIS is the surface geopotential. For identifying atmospheric rivers (ARs) we use the following TE commands, first detecting ridges in the IVT field, then filtering out points within 5 degrees great circle distance of TC features:

```
DetectBlobs
--thresholdcmd "_LAPLACIAN{8,10.0}(_VECMAG(TUQ,TVQ)),<=,-30000,0"
--minabslat 20
--geofiltercmd "area,>,850000km2"
--tagvar "AR_binary_tag"

NodeFileFilter
--bydist 5.0
--invert
--var "TC_binary_tag"
```


TUQ and TVQ are the zonal and meridional column-integrated moisture fluxes, respectively. For identifying extratropical cyclones (ETCs) we identify sea level pressure minima that do not possess an upper level warm core and traverse a sufficiently far distance over their lifetime:

```
DetectNodes
--searchbymin PSL
--closedcontourcmd "PSL,200.0,5.5,0"
--noclosedcontourcmd "_DIFF(Z300,Z500),-6.0,6.5,1.0" --mergedist 9.0
--outputcmd "PSL,min,0;U10,max,2;_DIV(PHIS,9.81),min,0"

StitchNodes
--in_fmt "lon,lat,slp,wind,zs"
--range 9.0
--mintime "24h"
--maxgap "1"
--min_endpoint_dist 12.0
```

Acknowledgments

This research was supported as part of the Energy Exascale Earth System Model (E3SM) project, funded by the U.S. Department of Energy, Office of Science, Office of Biological and Environmental Research (BER). The data were produced using resources of the Argonne Leadership Computing Facility at Argonne National Laboratory, which is supported by the Office of Science of the U.S. Department of Energy under contract DE-AC02-06CH11357. The data were produced using resources of the National Energy Research Scientific Computing Center, a DOE Office of Science User Facility supported by the Office of Science of the U.S. Department of Energy under Contract No. DE-AC02-05CH11231. The Pacific Northwest National Laboratory is operated for the U.S. DOE by Battelle Memorial Institute under contract DE-AC05-76RL01830. Work at LLNL was performed under the auspices of the U.S. Department of Energy by Lawrence Livermore National Laboratory under contract DE-AC52-07NA27344.LLNL-JRNL-825746. Author Rhoades was funded by the Office of Biological and Environmental Research of the U.S. Department of Energy within the Regional and Global Climate Modeling Program under the “the Calibrated and Systematic Characterization, Attribution and Detection of Extremes (CASCADE)” Science Focus Area (award no. DE-AC02-05CH11231). Authors Rhoades and Ullrich were funded by the project “A Framework for Improving Analysis and Modeling of Earth System and Intersectoral Dynamics at Regional Scales” (award no. DE-SC0016605). We acknowledge the World Climate Research Programme, which, through its Working Group on Coupled Modelling, coordinated and promoted CMIP6. We thank the climate modeling groups for producing and making available their model output, the Earth System Grid Federation (ESGF) for archiving the data and providing access, and the multiple funding agencies who support CMIP6 and ESGF. We thank DOE’s RGMA program area, the Data Management program, and NERSC for making this coordinated CMIP6 analysis activity possible.

Data Availability Statement

Complete native model output is archived on HPSS system at NERSC (National Energy Research Scientific Computing Center). The dataset is available through the DOE Earth System Grid Federation (ESGF; Cinquini et al., 2014) at https://esgf-node.llnl.gov/search/e3sm/?model_version=1_0. The output presented in this manuscript will be made available from <https://e3sm.org/data/get-e3sm-data/>. Some of the figures presented herein were generated in part using E3SM Diags (C. Zhang et al., 2022; C. J. Zhang et al., 2022). NCO (C. S. Zender, 2008; C. Zender et al., 2022) was used to generate climatologies and for data regridding.

References

- Ajibola, F. O., Zhou, B., Gnitou, G. T., & Onyejuruwa, A. (2020). Evaluation of the performance of CMIP6 HighResMIP on West African precipitation. *Atmosphere*, 11(10), 1–15. <https://doi.org/10.3390/atmos11101053>
- Akinsanola, A., Kooperman, K., Pendergrass, P., Hannah, H., & Reed, R. (2020). Seasonal representation of extreme precipitation indices over the United States in CMIP6 present-day simulations. *Environmental Research Letters*, 15(9), 094003. <https://doi.org/10.1088/1748-9326/ab92c1>
- Bacmeister, J. T., Wehner, M. F., Neale, R. B., Gettelman, A., Hannay, C., Lauritzen, P. H., et al. (2014). Exploratory high-resolution climate simulations using the community atmosphere model (CAM). *Journal of Climate*, 27(9), 3073–3099. <https://doi.org/10.1175/JCLI-D-13-00387.1>
- Bador, M., Boé, J., Terray, L., Alexander, L. V., Baker, A., Bellucci, A., et al. (2020). Impact of higher spatial atmospheric resolution on precipitation extremes over land in global climate models. *Journal of Geophysical Research: Atmospheres*, 125(13), 1–23. <https://doi.org/10.1029/2019JD032184>
- Balaguru, K., Leung, L. R., Van Roekel, L. P., Golaz, J., Ullrich, P. A., Caldwell, P. M., et al. (2020). Characterizing tropical cyclones in the energy Exascale earth system model version 1. *Journal of Advances in Modeling Earth Systems*, 12(8), 1–23. <https://doi.org/10.1029/2019ms002024>
- Benedict, I., Van Heerwaarden, C. C., Weerts, A. H., & Hazeleger, W. (2019). The benefits of spatial resolution increase in global simulations of the hydrological cycle evaluated for the Rhine and Mississippi basins. *Hydrology and Earth System Sciences*, 23(3), 1779–1800. <https://doi.org/10.5194/hess-23-1779-2019>
- Caldwell, P. M., Mametjanov, A., Tang, Q., Van Roekel, L. P., Golaz, J. C., Lin, W., et al. (2019). The DOE E3SM coupled model version 1: Description and results at high resolution. *Journal of Advances in Modeling Earth Systems*, 11(12), 4095–4146. <https://doi.org/10.1029/2019MS001870>
- Chang, P., Zhang, S., Danabasoglu, G., Yeager, S. G., Fu, H., Wang, H., et al. (2020). An unprecedented set of high-resolution earth system simulations for understanding multiscale interactions in climate variability and change. *Journal of Advances in Modeling Earth Systems*, 12(12), e2020MS002298. <https://doi.org/10.1029/2020MS002298>
- Cherchi, A., Fogli, P. G., Lovato, T., Peano, D., Iovino, D., Gualdi, S., et al. (2019). Global mean climate and main patterns of variability in the CMCC-CM2 coupled model. *Journal of Advances in Modeling Earth Systems*, 11(1), 185–209. <https://doi.org/10.1029/2018MS001369>
- Cinquini, L., Crichton, D., Mattmann, C., Harney, J., Shipman, G., Wang, F., et al. (2014). The Earth System Grid Federation: An open infrastructure for access to distributed geospatial data. *Future Generation Computer Systems*, 36, 400–417. <https://doi.org/10.1016/j.future.2013.07.002>
- Coles, S. G. (2001). *An introduction to statistical modeling of extreme values*. Springer.
- De Kauwe, M. G., Disney, M. I., Quaipe, T., Lewis, P., & Williams, M. (2011). An assessment of the MODIS collection 5 leaf area index product for a region of mixed coniferous forest. *Remote Sensing of Environment*, 115(2), 767–780. <https://doi.org/10.1016/j.rse.2010.11.004>
- Demory, M. E., Berthou, S., Fernández, J., Sørland, S. L., Brogli, R., Roberts, M. J., et al. (2020). European daily precipitation according to EURO-CORDEX regional climate models (RCMs) and high-resolution global climate models (GCMs) from the High-Resolution Model Intercomparison Project (HighResMIP). *Geoscientific Model Development*, 13(11), 5485–5506. <https://doi.org/10.5194/gmd-13-5485-2020>
- Demory, M. E., Vidale, P. L., Roberts, M. J., Berrisford, P., Strachan, J., Schiemann, R., & Mizielinski, M. S. (2014). The role of horizontal resolution in simulating drivers of the global hydrological cycle. *Climate Dynamics*, 42(7–8), 2201–2225. <https://doi.org/10.1007/s00382-013-1924-4>
- Dennis, J. M., Edwards, J., Evans, K. J., Guba, O., Lauritzen, P. H., Mirin, A. A., et al. (2012). CAM-SE: A scalable spectral element dynamical core for the community atmosphere model. *International Journal of High Performance Computing Applications*, 26(1), 74–89. <https://doi.org/10.1177/1094342011428142>

- Eyring, V., Bony, S., Meehl, G. A., Senior, C. A., Stevens, B., Stouffer, R. J., & Taylor, K. E. (2016). Overview of the coupled model Intercomparison project phase 6 (CMIP6) experimental design and organization. *Geoscientific Model Development*, 9(5), 1937–1958. <https://doi.org/10.5194/gmd-9-1937-2016>
- Gent, P. R., & McWilliams, J. C. (1990). Isopycnal mixing in ocean circulation models. *Journal of Physical Oceanography*, 20(1), 150–155. [https://doi.org/10.1175/1520-0485\(1990\)020<0150:IMIOCM>2.0.CO;2](https://doi.org/10.1175/1520-0485(1990)020<0150:IMIOCM>2.0.CO;2)
- Gottelman, A., & Morrison, H. (2015). Advanced two-moment bulk microphysics for global models. Part I: Off-line tests and comparison with other schemes. *Journal of Climate*, 28(3), 1268–1287. <https://doi.org/10.1175/JCLI-D-14-00102.1>
- Gottelman, A., Morrison, H., Santos, S., Bogenschütz, P., & Caldwell, P. M. (2015). Advanced two-moment bulk microphysics for global models. Part II: Global model solutions and aerosol-cloud interactions. *Journal of Climate*, 28(3), 1288–1307. <https://doi.org/10.1175/JCLI-D-14-00103.1>
- Golaz, J., Caldwell, P. M., Van Roekel, L. P., Petersen, M. R., Tang, Q., Wolfe, J. D., et al. (2019). The DOE E3SM coupled model version 1: Overview and evaluation at standard resolution. *Journal of Advances in Modeling Earth Systems*, 11(7), 2089–2129. <https://doi.org/10.1029/2018ms001603>
- Golaz, J.-C., Larson, V. E., & Cotton, W. R. (2002). A PDF-based model for boundary layer clouds. Part I: Method and model description. *Journal of the Atmospheric Sciences*, 59(24), 3540–3551. [https://doi.org/10.1175/1520-0469\(2002\)059<3540:APBMFB>2.0.CO;2](https://doi.org/10.1175/1520-0469(2002)059<3540:APBMFB>2.0.CO;2)
- Gutjahr, O., Putrasahan, D., Lohmann, K., Jungclaus, J. H., Von Storch, J. S., Brüggemann, N., et al. (2019). Max Planck Institute earth system model (MPI-ESM1.2) for the high-resolution model Intercomparison project (HighResMIP). *Geoscientific Model Development*, 12(7), 3241–3281. <https://doi.org/10.5194/gmd-12-3241-2019>
- Haarsma, R. J., Roberts, M. J., Vidale, P. L., Catherine, A., Bellucci, A., Bao, Q., et al. (2016). High resolution model Intercomparison project (HighResMIP v1.0) for CMIP6. *Geoscientific Model Development*, 9(11), 4185–4208. <https://doi.org/10.5194/gmd-9-4185-2016>
- Harrop, B. E., Ma, P., Rasch, P. J., Qian, Y., Lin, G., & Hannay, C. (2019). Understanding monsoonal water cycle changes in a warmer climate in E3SMv1 using a normalized gross moist stability framework. *Journal of Geophysical Research: Atmospheres*, 124(20), 10826–10843. <https://doi.org/10.1029/2019JD031443>
- He, C., Chen, F., Barlage, M., Liu, C., Newman, A., Tang, W., et al. (2019). Can convection-permitting modeling provide decent precipitation for offline high-resolution snowpack simulations over mountains? *Journal of Geophysical Research: Atmospheres*, 124(23), 12631–12654. <https://doi.org/10.1029/2019JD030823>
- Hersbach, H., Bell, B., Berrisford, P., Hirahara, S., Horányi, A., Muñoz-Sabater, J., et al. (2020). The ERA5 global reanalysis. *Quarterly Journal of the Royal Meteorological Society*, 146(730), 1999–2049. <https://doi.org/10.1002/qj.3803>
- Hobeichi, S., Abramowitz, G., Evans, J., & Ukkola, A. (2018). Derived optimal linear combination evapotranspiration (DOLCE): A global gridded synthesis ET estimate. *Hydrology and Earth System Sciences*, 22(2), 1317–1336. <https://doi.org/10.5194/hess-22-1317-2018>
- Huang, F., Xu, Z., & Guo, W. (2020). The linkage between CMIP5 climate models' abilities to simulate precipitation and vector winds. *Climate Dynamics*, 54(11–12), 4953–4970. <https://doi.org/10.1007/s00382-020-05259-6>
- Huang, X., & Ullrich, P. A. (2017). The changing character of twenty-first-century precipitation over the western United States in the variable-resolution CESM. *Journal of Climate*, 30(18), 7555–7575. <https://doi.org/10.1175/JCLI-D-16-0673.1>
- Huffman, G. J., Adler, R. F., Bolvin, D. T., & Gu, G. (2009). Improving the global precipitation record: GPCP version 2.1. *Geophysical Research Letters*, 36(17), 701. <https://doi.org/10.1029/2009gl040000>
- Huffman, G. J., Adler, R. F., Bolvin, D. T., Gu, G., Nelkin, E. J., Bowman, K. P., et al. (2007). The TRMM Multisatellite Precipitation Analysis (TMPA): Quasi-global, multiyear, combined-sensor precipitation estimates at fine scales. *Journal of Hydrometeorology*, 8(1), 38–55. <https://doi.org/10.1175/JHM560.1>
- Huffman, G. J., Adler, R. F., Morrissey, M. M., Bolvin, D. T., Curtis, S., Joyce, R., et al. (2001). Global precipitation at one-degree daily resolution from multisatellite observations. *Journal of Hydrometeorology*, 2(1), 36–50. [https://doi.org/10.1175/1525-7541\(2001\)002<0036:GPAODD>2.0.CO;2](https://doi.org/10.1175/1525-7541(2001)002<0036:GPAODD>2.0.CO;2)
- Iacono, M. J., Delamere, J. S., Mlawer, E. J., Shephard, M. W., Clough, S. A., & Collins, W. D. (2008). Radiative forcing by long-lived greenhouse gases: Calculations with the AER radiative transfer models. *Journal of Geophysical Research*, 113(D13), D13103. <https://doi.org/10.1029/2008JD009944>
- Iorio, J. P., Duffy, P. B., Govindasamy, B., Thompson, S. L., Khairoutdinov, M., & Randall, D. (2004). Effects of model resolution and subgrid-scale physics on the simulation of precipitation in the continental United States. *Climate Dynamics*, 23(3–4), 243–258. <https://doi.org/10.1007/s00382-004-0440-y>
- Ito, R., Nakaegawa, T., & Takayabu, I. (2020). Comparison of regional characteristics of land precipitation climatology projected by an MRI-AGCM multi-cumulus scheme and multi-SST ensemble with CMIP5 multi-model ensemble projections. *Progress in Earth and Planetary Science*, 7(1), 77. <https://doi.org/10.1186/s40645-020-00394-4>
- Jagannathan, K., Jones, A. D., & Ray, I. (2020). The making of a metric: Co-Producing decision-relevant climate science. *Bulletin of the American Meteorological Society*, 102(8), 1–33. <https://doi.org/10.1175/BAMS-D-19-0296.1>
- Jung, T., Miller, M. J., Palmer, T. N., Towers, P., Wedi, N., Achuthavarier, D., et al. (2012). High-resolution global climate simulations with the ECMWF model in project athena: Experimental design, model climate, and seasonal forecast skill. *Journal of Climate*, 25(9), 3155–3172. <https://doi.org/10.1175/JCLI-D-11-00265.1>
- Kiehl, J. T., & Williamson, D. L. (1991). Dependence of cloud amount on horizontal resolution in the National center for atmospheric research community climate model. *Journal of Geophysical Research*, 96(D6), 10955–10980. <https://doi.org/10.1029/91jd00164>
- Krinner, G., Derksen, C., Essery, R., Flanner, M., Hagemann, S., Clark, M., et al. (2018). ESM-SnowMIP: Assessing snow models and quantifying snow-related climate feedbacks. *Geoscientific Model Development*, 11(12), 5027–5049. <https://doi.org/10.5194/gmd-11-5027-2018>
- Larson, V. E. (2017). CLUBB-SILHS: A parameterization of subgrid variability in the atmosphere. *arXiv*.
- Larson, V. E., & Golaz, J.-C. (2005). Using probability density functions to derive consistent closure relationships among higher-order moments. *Monthly Weather Review*, 133(4), 1023–1042. <https://doi.org/10.1175/MWR2902.1>
- Leung, L. R., Bader, D. C., Taylor, M. A., & McCoy, R. B. (2020). An introduction to the E3SM special collection: Goals, science drivers, development, and analysis. *Journal of Advances in Modeling Earth Systems*, 12(11), e2019MS001821. <https://doi.org/10.1029/2019ms001821>
- Li, H., Wigmosta, M. S., Wu, H., Huang, M., Ke, Y., Coleman, A. M., & Leung, L. R. (2013). A physically based runoff routing model for land surface and earth system models. *Journal of Hydrometeorology*, 14(3), 808–828. <https://doi.org/10.1175/JHM-D-12-015.1>
- Li, H. Y., Leung, L. R., Getirana, A., Huang, M., Wu, H., Xu, Y., et al. (2015). Evaluating global streamflow simulations by a physically based routing model coupled with the community land model. *Journal of Hydrometeorology*, 16(2), 948–971. <https://doi.org/10.1175/JHM-D-14-0079.1>
- Lian, X., Piao, S., Huntingford, C., Li, Y., Zeng, Z., Wang, X., et al. (2018). Partitioning global land evapotranspiration using CMIP5 models constrained by observations. *Nature Climate Change*, 8(7), 640–646. <https://doi.org/10.1038/s41558-018-0207-9>

- Liu, X., Ma, P. L., Wang, H., Tilmes, S., Singh, B., Easter, R. C., et al. (2016). Description and evaluation of a new four-mode version of the modal aerosol module (MAM4) within version 5.3 of the community atmosphere model. *Geoscientific Model Development*, 9(2), 505–522. <https://doi.org/10.5194/gmd-9-505-2016>
- Livneh, B., & Badger, A. M. (2020). Drought less predictable under declining future snowpack. *Nature Climate Change*, 10(5), 452–458. <https://doi.org/10.1038/s41558-020-0754-8>
- Livneh, B., Rosenberg, E. A., Lin, C., Nijssen, B., Mishra, V., Andreadis, K. M., et al. (2013). A long-term hydrologically based dataset of land surface fluxes and states for the conterminous United States: Update and extensions. *Journal of Climate*, 26(23), 9384–9392. <https://doi.org/10.1175/JCLI-D-12-00508.1>
- Lynn, E., Cuthbertson, A., He, M., Vasquez, J. P., Anderson, M. L., Coombe, P., et al. (2020). Technical note: Precipitation-phase partitioning at landscape scales to regional scales. *Hydrology and Earth System Sciences*, 24(11), 5317–5328. <https://doi.org/10.5194/hess-24-5317-2020>
- Mahajan, S., Evans, K. J., Branstetter, M., Anantharaj, V., & Leifeld, J. K. (2015). Fidelity of precipitation extremes in high resolution global climate simulations. *Procedia Computer Science*, 51(1), 2178–2187. <https://doi.org/10.1016/j.procs.2015.05.492>
- Mahajan, S., Evans, K. J., Branstetter, M. L., & Tang, Q. (2018). Model resolution sensitivity of the simulation of North Atlantic oscillation teleconnections to precipitation extremes. *Journal of Geophysical Research: Atmospheres*, 123(20), 11392–11409. <https://doi.org/10.1029/2018JD028594>
- Mahajan, S., Tang, Q., Keen, N. D., Golaz, J. C., & van Roekel, L. P. (2022). Simulation of ENSO teleconnections to precipitation extremes over the United States in the high-resolution version of E3SM. *Journal of Climate*, 35(11), 3371–3393. <https://doi.org/10.1175/JCLI-D-20-1011.1>
- Margulis, S. A., Cortés, G., Giroto, M., & Durand, M. (2016). A landsat-era sierra Nevada snow reanalysis (1985–2015). *Journal of Hydrometeorology*, 17(4), 1203–1221. <https://doi.org/10.1175/JHM-D-15-0177.1>
- Martens, B., Miralles, D. G., Lievens, H., Van Der Schalie, R., De Jeu, R. A., Fernández-Prieto, D., et al. (2017). GLEAM v3: Satellite-based land evaporation and root-zone soil moisture. *Geoscientific Model Development*, 10(5), 1903–1925. <https://doi.org/10.5194/gmd-10-1903-2017>
- McCrary, R. R., McGinnis, S., & Mearns, L. O. (2017). Evaluation of snow water equivalent in NARCCAP simulations, including measures of observational uncertainty. *Journal of Hydrometeorology*, 18(9), 2425–2452. <https://doi.org/10.1175/JHM-D-16-0264.1>
- Miralles, D. G., Holmes, T. R., De Jeu, R. A., Gash, J. H., Meesters, A. G., & Dolman, A. J. (2011). Global land-surface evaporation estimated from satellite-based observations. *Hydrology and Earth System Sciences*, 15(2), 453–469. <https://doi.org/10.5194/hess-15-453-2011>
- Mlawer, E. J., Taubman, S. J., Brown, P. D., Iacono, M. J., & Clough, S. A. (1997). Radiative transfer for inhomogeneous atmospheres: RRTM, a validated correlated-k model for the longwave. *Journal of Geophysical Research*, 102(D14), 16663–16682. <https://doi.org/10.1029/97JD00237>
- Monerie, P. A., Chevuturi, A., Cook, P., Klingaman, N. P., & Holloway, C. E. (2020). Role of atmospheric horizontal resolution in simulating tropical and subtropical South American precipitation in HadGEM3-GC3.1. *Geoscientific Model Development*, 13(10), 4749–4771. <https://doi.org/10.5194/gmd-13-4749-2020>
- Mote, P. W., Li, S., Lettenmaier, D. P., Xiao, M., & Engel, R. (2018). Dramatic declines in snowpack in the western US. *npj Climate and Atmospheric Science*, 1(1), 2. <https://doi.org/10.1038/s41612-018-0012-1>
- Mu, Q., Zhao, M., & Running, S. W. (2011). Improvements to a MODIS global terrestrial evapotranspiration algorithm. *Remote Sensing of Environment*, 115(8), 1781–1800. <https://doi.org/10.1016/j.rse.2011.02.019>
- Neale, R. B., Richter, J. H., & Jochum, M. (2008). The impact of convection on ENSO: From a delayed oscillator to a series of events. *Journal of Climate*, 21(22), 5904–5924. <https://doi.org/10.1175/2008JCLI2244.1>
- Oleson, K. W., Lawrence, D. M., Bonan, G. B., Drevniak, B., Huang, M., Koven, C. D., et al. (2013). Technical description of version 4.5 of the community land model (CLM). In *NCAR/TN-478+STR NCAR technical note (April)*, 266. <https://doi.org/10.5065/D6RR1W7M>
- Pendergrass, A. G., Gleckler, P., Leung, L. R., & Jakob, C. (2020). Benchmarking simulated precipitation in earth system models. *Bulletin of the American Meteorological Society*, 101(6), E814–E816. <https://doi.org/10.1175/bams-d-19-0318.1>
- Pendergrass, A. G., & Knutti, R. (2018). The uneven nature of daily precipitation and its change. *Geophysical Research Letters*, 45(21), 1–9. <https://doi.org/10.1029/2018GL080298>
- Petersen, M. R., Asay-Davis, X. S., Berres, A. S., Chen, Q., Feige, N., Hoffman, M. J., et al. (2019). An evaluation of the ocean and Sea Ice climate of E3SM using MPAS and interannual CORE-II forcing. *Journal of Advances in Modeling Earth Systems*, 11(5), 1438–1458. <https://doi.org/10.1029/2018MS001373>
- Rasch, P. J., Xie, S., Ma, P. L., Lin, W., Wang, H., Tang, Q., et al. (2019). An overview of the atmospheric component of the energy Exascale earth system model. *Journal of Advances in Modeling Earth Systems*, 11(8), 2377–2411. <https://doi.org/10.1029/2019MS001629>
- Rhoades, A. M., Jones, A. D., O'Brien, T. A., O'Brien, J. P., Ullrich, P. A., & Zarzycki, C. M. (2020a). Influences of North Pacific ocean domain extent on the western U.S. Winter hydroclimatology in variable-resolution CESM. *Journal of Geophysical Research: Atmospheres*, 125(14). <https://doi.org/10.1029/2019JD031977>
- Rhoades, A. M., Jones, A. D., Srivastava, A., Huang, H., O'Brien, T. A., Patricola, C. M., et al. (2020b). The shifting scales of western U.S. Landfalling atmospheric rivers under climate change. *Geophysical Research Letters*, 47(17), 1–14. <https://doi.org/10.1029/2020GL089096>
- Rhoades, A. M., Jones, A. D., & Ullrich, P. A. (2018a). Assessing mountains as natural reservoirs with a multimetric framework. *Earth's Future*, 6(9), 1221–1241. <https://doi.org/10.1002/2017EF000789>
- Rhoades, A. M., Jones, A. D., & Ullrich, P. A. (2018b). The changing character of the California sierra Nevada as a natural reservoir. *Geophysical Research Letters*, 45(23), 13008–13019. <https://doi.org/10.1029/2018GL080308>
- Rhoades, A. M., Risser, M. D., Stone, D. A., Wehner, M. F., & Jones, A. D. (2021). Implications of warming on western United States landfalling atmospheric rivers and their flood damages. *Weather and Climate Extremes*, 32(March), 100326. <https://doi.org/10.1016/j.wace.2021.100326>
- Richter, J. H., & Rasch, P. J. (2008). Effects of convective momentum transport on the atmospheric circulation in the community atmosphere model, version 3. *Journal of Climate*, 21(7), 1487–1499. <https://doi.org/10.1175/2007JCLI1789.1>
- Ringler, T., Petersen, M., Higdun, R. L., Jacobsen, D., Jones, P. W., & Maltrud, M. (2013). A multi-resolution approach to global ocean modeling. *Ocean Modelling*, 69, 211–232. <https://doi.org/10.1016/j.ocemod.2013.04.010>
- Roberts, C. D., Senan, R., Molteni, F., Boussetta, S., Mayer, M., & Keeley, S. P. (2018). Climate model configurations of the ECMWF integrated forecasting system (ECMWF-IFS cycle 43r1) for HighResMIP. *Geoscientific Model Development*, 11(9), 3681–3712. <https://doi.org/10.5194/gmd-11-3681-2018>
- Roberts, M. J., Baker, A., Blockley, E. W., Calvert, D., Coward, A., Hewitt, H. T., et al. (2019). Description of the resolution hierarchy of the global coupled HadGEM3-GC3.1 model as used in CMIP6 HighResMIP experiments. *Geoscientific Model Development*, 12(12), 4999–5028. <https://doi.org/10.5194/gmd-12-4999-2019>
- Routson, C. C., McKay, N. P., Kaufman, D. S., Erb, M. P., Goosse, H., Shuman, B. N., et al. (2019). Mid-latitude net precipitation decreased with Arctic warming during the Holocene. *Nature*, 568(7750), 83–87. <https://doi.org/10.1038/s41586-019-1060-3>

- Schiemann, R., Luigi Vidale, P., Shaffrey, L. C., Johnson, S. J., Roberts, M. J., Demory, M. E., et al. (2018). Mean and extreme precipitation over European river basins better simulated in a 25 km AGCM. *Hydrology and Earth System Sciences*, 22(7), 3933–3950. <https://doi.org/10.5194/hess-22-3933-2018>
- Seaber, P., Kapinos, F., & Knapp, G. (1987). Hydrologic Unit Maps: U.S. Geological Survey Water-Supply Paper 2294. Retrieved from http://pubs.usgs.gov/wsp/wsp2294/pdf/wsp_2294.pdf
- Sharma, A., Hamlet, A. F., & Fernando, H. J. (2019). Lessons from inter-comparison of decadal climate simulations and observations for the midwest U.S. And great Lakes region. *Atmosphere*, 10(5), 266. <https://doi.org/10.3390/atmos10050266>
- Siirila-Woodburn, E., Rhoades, A. M., Hatchett, B. J., Huning, L., Szinai, J., Tague, C., et al. (2021). A low-to-no snow future and its impacts on water resources in the western United States. *Nature Reviews Earth & Environment*, 2(11), 800–819. <https://doi.org/10.1038/s43017-021-00219-y>
- Small, R. J., Bacmeister, J., Bailey, D., Baker, A., Bishop, S., Bryan, F., et al. (2014). A new synoptic scale resolving global climate simulation using the Community Earth System Model. *Journal of Advances in Modeling Earth Systems*, 6(4), 1065–1094. <https://doi.org/10.1002/2014MS000363>
- Srivastava, A., Grotjahn, R., & Ullrich, P. (2020). Evaluation of historical CMIP6 model simulations of extreme precipitation over contiguous US regions. *Weather and Climate Extremes*, 29(December 2019), 100268. <https://doi.org/10.1016/j.wace.2020.100268>
- Stephens, G. L., L'Ecuyer, T., Forbes, R., Gettleman, A., Golaz, J. C., Bodas-Salcedo, A., et al. (2010). Dreary state of precipitation in global models. *Journal of Geophysical Research*, 115(24), 1–14. <https://doi.org/10.1029/2010JD014532>
- Stevens, B., Satoh, M., Auger, L., Biercamp, J., Bretherton, C. S., Chen, X., et al. (2019). DYAMOND: The DYNAMics of the atmospheric general circulation modeled on non-hydrostatic Domains. *Progress in Earth and Planetary Science*, 6(1), 61. <https://doi.org/10.1186/s40645-019-0304-z>
- Sturm, M., Goldstein, M. A., & Parr, C. (2017). Water and life from snow: A trillion dollar science question. *Water Resources Research*, 53(5), 3534–3544. <https://doi.org/10.1002/2017WR020840>
- Swenson, S., & Wahr, J. (2006). Post-processing removal of correlated errors in GRACE data. *Geophysical Research Letters*, 33(8), 1–4. <https://doi.org/10.1029/2005GL025285>
- Tang, Q., Golaz, J.-C., Van Roekel, L. P., Taylor, M. A., Lin, W., Hillman, B. R., et al. (2022). The fully coupled regionally refined model of E3SM version 2: Overview of the atmosphere, land, and river. In *Geoscientific model development discussions* (pp. 1–64). <https://doi.org/10.5194/gmd-2022-262>
- Tang, Q., Klein, S. A., Xie, S., Lin, W., Golaz, J. C., Roesler, E. L., et al. (2019). Regionally refined test bed in E3SM atmosphere model version 1 (EAMv1) and applications for high-resolution modeling. *Geoscientific Model Development*, 12(7), 2679–2706. <https://doi.org/10.5194/gmd-12-2679-2019>
- Taylor, K. E., Stouffer, R. J., & Meehl, G. A. (2012). An overview of CMIP5 and the experiment design. *Bulletin of the American Meteorological Society*, 93(4), 485–498. <https://doi.org/10.1175/BAMS-D-11-00094.1>
- Terai, C. R., Caldwell, P. M., Klein, S. A., Tang, Q., & Branstetter, M. L. (2017). The atmospheric hydrologic cycle in the ACME v0.3 model. *Climate Dynamics*, 0(0), 1–29. <https://doi.org/10.1007/s00382-017-3803-x>
- Trujillo, E., & Molotch, N. P. (2014). Snowpack regimes of the western United States. *Water Resources Research*, 50(7), 5611–5623. <https://doi.org/10.1002/2013WR014753>
- Ullrich, P. A. (2021). TempestExtremes user guide. Retrieved from <https://climate.ucdavis.edu/tempestextremes.php>
- Ullrich, P. A., Devendran, D., & Johansen, H. (2016). Arbitrary-order conservative and consistent remapping and a theory of linear maps: Part II. *Monthly Weather Review*, 144(4), 1529–1549. <https://doi.org/10.1175/MWR-D-15-0301.1>
- Ullrich, P. A., & Taylor, M. A. (2015). Arbitrary-order conservative and consistent remapping and a theory of linear maps: Part I. *Monthly Weather Review*, 143(6), 2419–2440. <https://doi.org/10.1175/MWR-D-14-00343.1>
- Ullrich, P. A., Zarzycki, C. M., McClenny, E. E., Pinheiro, M. C., Stansfield, A. M., & Reed, K. A. (2021). Tempestextremes v2.1: A community framework for feature detection, tracking and analysis in large datasets. In *Geoscientific model development discussions* (pp. 1–37).
- Vannière, B., Demory, M. E., Vidale, P. L., Schiemann, R., Roberts, M. J., Roberts, C. D., et al. (2019). Multi-model evaluation of the sensitivity of the global energy budget and hydrological cycle to resolution. *Climate Dynamics*, 52(11), 6817–6846. <https://doi.org/10.1007/s00382-018-4547-y>
- Wang, H., Easter, R. C., Zhang, R., Ma, P.-L., Singh, B., Zhang, K., et al. (2020). Aerosols in the E3SM version 1: New developments and their impacts on radiative forcing. *Journal of Advances in Modeling Earth Systems*, 12(1), e2019MS001851. <https://doi.org/10.1029/2019MS001851>
- Wehner, M., Lee, J., Risser, M., Ullrich, P., Gleckler, P., & Collins, W. D. (2021). Evaluation of extreme sub-daily precipitation in high-resolution global climate model simulations. *Philosophical transactions. Series A, Mathematical, physical, and engineering sciences*, 379(2195), 20190545. <https://doi.org/10.1098/rsta.2019.0545>
- Wehner, M. F., Reed, K. A., Li, F., Bacmeister, J., Chen, C.-T., et al. (2014). The effect of horizontal resolution on simulation quality in the Community Atmospheric Model, CAM5.1. *Journal of Advances in Modeling Earth Systems*, 6(4), 980–997. <https://doi.org/10.1002/2013MS000276>
- Wehner, M. F., Smith, R. L., Bala, G., & Duffy, P. (2010). The effect of horizontal resolution on simulation of very extreme US precipitation events in a global atmosphere model. *Climate Dynamics*, 34(2), 241–247. <https://doi.org/10.1007/s00382-009-0656-y>
- Xie, S., Lin, W., Rasch, P. J., Ma, P.-L., Neale, R., Larson, V. E., et al. (2018). Understanding cloud and convective characteristics in version 1 of the E3SM Atmosphere Model. *Journal of Advances in Modeling Earth Systems*, 10(10), 2618–2644. <https://doi.org/10.1029/2018ms001350>
- Xu, Y., Jones, A., & Rhoades, A. (2019). A quantitative method to decompose SWE differences between regional climate models and reanalysis datasets. *Scientific Reports*, 9(1), 16520. <https://doi.org/10.1038/s41598-019-52880-5>
- Zamuda, C., Mignone, B., Bilello, D., Hallett, K., Lee, C., Macknick, J., et al. (2013). U.S. Energy sector vulnerabilities to climate change and extreme weather (technical report). Retrieved from <http://energy.gov/downloads/us-energy-sector-vulnerabilities-climate-change-and-extreme-weather>
- Zender, C., Vicente, P., Wang, D. L., Wenshanw, J. M., et al. (2022). nco/nco: Rattlesnake. *Zenodo*. <https://doi.org/10.5281/zenodo.595745>
- Zender, C. S. (2008). Analysis of self-describing gridded geoscience data with NETCDF operators (NCO). *Environmental Modelling & Software*, 23(10), 1338–1342. <https://doi.org/10.1016/j.envsoft.2008.03.004>
- Zhang, C., Golaz, J.-C., Forsyth, R., Vo, T., Xie, S., Shaheen, Z., et al. (2022). The E3SM diagnostics package (E3SM diags v2.7): A python-based diagnostics package for earth system models evaluation. In *Geoscientific model development discussions* (pp. 1–35). <https://doi.org/10.5194/gmd-2022-38>
- Zhang, C. J., Golaz, C., Forsyth, R., Vo, T., Asay-Davis, X., Bradley, A. M., & Shaheen, Z. (2022). E3sm-project/e3sm_diags: v2.7.0. *Zenodo*. <https://doi.org/10.5281/zenodo.6819849>

- Zhang, G. J., & McFarlane, N. A. (1995). Sensitivity of climate simulations to the parameterization of cumulus convection in the Canadian climate centre general circulation model. *Atmosphere-Ocean*, *33*(3), 407–446. <https://doi.org/10.1080/07055900.1995.9649539>
- Zhang, L., Wu, P., Zhou, T., Roberts, M. J., & Schiemann, R. (2016). Added value of high resolution models in simulating global precipitation characteristics. *Atmospheric Science Letters*, *17*(12), 646–657. <https://doi.org/10.1002/asl.715>